

ALMA MATER STUDIORUM · UNIVERSITÀ DI BOLOGNA

Scuola di Scienze
Dipartimento di Fisica e Astronomia
Corso di Laurea in Fisica

The Inverse Kinematics approach in the FOOT experiment

Relatore:
Chiar.mo Prof. Antonio Zoccoli

Presentata da:
Celeste Ottaviani

Correlatore:
Dott. Roberto Spighi

Anno Accademico 2017/2018

Sommario

La presente tesi si propone di fornire una descrizione approfondita dell'approccio della Cinematica Inversa applicata all'esperimento FOOT (FragmentatiOn Of Target). Tale esperimento è stato sviluppato con lo scopo di migliorare la conoscenza dell'efficacia biologica degli ioni impiegati nella cura delle neoplasie tramite la misura delle sezioni d'urto differenziali dei processi di frammentazione nucleare che si verificano nei trattamenti di adroterapia. Tuttavia, nella pratica sperimentale si presenta l'impossibilità di ottenere queste misure; i frammenti generati nella disintegrazione dei nuclei nei tessuti del paziente hanno energia cinetica molto bassa e rimangono intrappolati nel bersaglio senza poter essere rivelati dall'apparato. Una possibile soluzione consiste nell'impiegare un bersaglio a bassa densità (al limite gassoso), con spessore micrometrico. Questo, però, comporterebbe una drastica riduzione della probabilità di interazione e lunghi tempi di presa dati. FOOT utilizza, invece, un approccio di cinematica inversa che permette l'inversione dei ruoli di fascio e bersaglio; la frammentazione del bersaglio viene infatti studiata utilizzando fasci di nuclei pesanti contro bersagli ricchi di idrogeno e applicando successivamente una trasformazione di Lorentz ai frammenti prodotti. Questa stessa tecnica si estende anche al caso in cui il proiettile sia costituito da nuclei pesanti che, invece, favoriscono la frammentazione sia del fascio che del bersaglio.

Lo scopo del lavoro di tesi consiste, pertanto, nel fornire un resoconto completo e dettagliato della Cinematica Inversa sopperendo alla mancanza di documentazione sull'argomento. Sono stati delineati i problemi sperimentali, i vantaggi derivanti dall'applicazione di questa tecnica e si è accennato alla struttura matematica di base. Si è mostrata inoltre la validità dell'approccio confrontando plot di distribuzione di energia cinetica di frammenti ottenuti da simulazioni in cinematica diretta ed inversa.

Abstract

This thesis is intended to provide an in-depth description of the Inverse Kinematics approach applied to the FOOT (FragmentatiOn Of Target) experiment. This experiment was developed with the goal of improving the knowledge of the biological effectiveness of ions employed in the neoplasms treatment through the measurement of the differential cross section of the nuclear fragmentation processes that take place during hadrontherapy. However, in the experimental practice arises the inability of obtaining these measurements; the fragments produced in the patient's tissues disintegration have a really low kinetic energy and remain trapped inside the target without possibility of being detected. A possible solution consists in the employment of a low density target (even gaseous), with a micrometric thickness; however, this would cause a drastic reduction of the interaction probability and the required times for the data taking would be extremely long. Therefore, FOOT takes advantage of an Inverse Kinematic approach in which the projectile and target roles are switched; this way the target fragmentation can be studied with the use of heavy ions beams against enriched Hydrogen targets and successively applying a Lorentz boost on the produced fragments. This same approach can be extended to the case in which the beam is made up of heavy nuclei that, in the collision, cause the production of both beam and target fragments.

The present thesis therefore supplies a complete and detailed report of the Inverse Kinematics providing for the lack of a good formulation of this topic. In this work, the experimental problems and the advantages deriving from the application of this method were delineated along with the basic mathematical structure. It has been shown the validity of this approach through the comparison of kinetic energy distributions for the fragments, obtained from simulated interactions in direct and inverse kinematics.

Contents

Introduction	9
1 Ionizing radiations in medical treatments	11
1.1 Biological effects of Radiation	11
1.1.1 Radiation induced damage	11
1.1.2 Absorbed Dose	13
1.1.3 Linear Energy Transfer	13
1.1.4 Relative Biological Effectiveness	14
1.1.5 Oxygen Enhancement Ratio	15
1.2 Interaction of Heavy Charged Particles with Matter	17
1.2.1 The Bethe-Bloch formula and Stopping Power	17
1.2.2 Range	19
1.2.3 Multiple Scattering	20
1.2.4 Nuclear Fragmentation	21
1.3 Application in Cancer Treatment	24
1.3.1 Radiotherapy	24
1.3.2 Hadrontherapy	26
1.4 Proton RBE	30
2 The FOOT Experiment	33
2.1 The aim of the experiment	34
2.1.1 Target fragmentation and RBE variability	34
2.1.2 Projectile fragmentation for Carbon beams	34
2.1.3 Projectile fragmentation for Oxygen beams	34
2.1.4 Projectile fragmentation for Helium beams	34
2.1.5 Radioprotection in Space	35
2.2 The experimental setup	36
2.2.1 Start Counter	36
2.2.2 Beam Monitor	37
2.2.3 Fragments detection setup	39
2.3 Experimental goals and requirements	46
2.4 Fragments identification and measured quantities	46

3 Inverse Kinematics	49
3.1 Abrasion/Ablation Model for Nuclear Fragmentation	49
3.1.1 Fragmentation Cross Sections	50
3.2 Projectile and Target fragmentation	52
3.3 Target material	53
3.4 Mathematical Formulation of the Inverse Kinematics	55
3.4.1 Application	57
3.5 Fragments characteristics in Direct and Inverse Kinematics	58
Conclusions	67
Bibliography	69

Introduction

The word *cancer* is derived from the Latin word for crab because this pathology shares with this animal the capability of grabbing and being persistent; in fact, this disease shows a high endurance to therapies and medical treatments. It is one of the major widespread health problems and a leading cause of death worldwide. The cancer is a neoplasm, an abnormal growth of cells that exhibits a functionality variation and an abnormal differentiation. It causes a more rapid development of the cells compared to the normal behavior and induces a continuous spreading of the anomaly. During their growth, neoplasms have the ability to invade surrounding tissues causing metastasis, expansions of the tumor from the primary site of development to a secondary site [1].

There are numerous therapies involved in cancer treatment, but this thesis will address specifically the Hadrontherapy, also called Ion Beam Therapy. It takes advantage of high-energy beams of charged particles, protons (60-250 MeV) and heavier ions (100-400 MeV per nucleon), to reach deep tumors.

Hadrontherapy had a rapid development and diffusion in recent years due to the progresses in technology and radiation oncology techniques. It represents a valid alternative to the conventional radiotherapy that uses photons or, more rarely, electrons.

Comparing these therapies, the main advantage of the hadrontherapy with respect to the radiotherapy lies in the different energy loss mechanism. The dose release profile of radiation with photons presents a dose peak at short distance from the patient's skin followed by a decreasing release of the radiation in accordance with the absorption law. Since tumors are usually located in depth, the peak does not coincide with the cancer position and, consequently, the healthy tissues absorb a high fraction of the released dose and are subjected to an increased risk of damages. Hadrontherapy, on the other hand, presents a low dose profile at the beginning of the path and a sharp maximum - *Bragg peak* - near the end, whose depth depends on the beam energy. This treatment provides a high irradiation accuracy of the tumor volume and a reduced damage to the surrounding healthy tissues. The particles involved in this therapy present a high biological effectiveness, the capability of inducing a direct damage to the DNA of cancerous cells, that is even more enhanced in the case of beams of heavy ions (Carbon, Oxygen, ...). However, unfortunately, when using these beams, there is a major increase in the presence of fragments derived from the nuclear interactions of the beam and the patient tissues. Consequently, there is the release of a non-negligible dose in the entry region and beyond the Bragg peak, still not completely studied. Proton treatments are the most widespread but even in their employment occurs the problem of the fragmentation, that, in this specific case, concerns the target nuclei. This effect is relevant in the assessment of the correct biological effectiveness, influenced by the unevenness of the dose release; a precise knowledge of the fragmentation process is required to avoid an underestimation of the deposited dose in the healthy tissue region.

The FOOT (FragmentatiOn Of Target) experiment was designed with the purpose of providing for the lack of experimental measurements of nuclear reaction cross sections for fragments produced in the interaction between tissue nuclei and charged particles of the beam. One of its tasks is the study of both projectile and target fragmentation where the latter was almost completely neglected by previous experiments. These processes hold a great importance in the correct radiobiological characterization of hadrons and in the precise evaluation of induced

damage in the patient tissues.

Important issue of the target fragmentation is the low range (order of tens of microns) of the produced fragments that leaves them without any probability of escaping the target and, hence, to be detected. The solution of this problem, adopted in the FOOT experiment, is the application of the *Inverse Kinematic approach* in which the role of the projectile and target are reversed.

The Inverse Kinematics approach represents the central point of this thesis that is intended to deepen this topic that covers a relevant role in the study of nuclear fragmentation in the case of a beam of light particles impinging on a target of heavy nuclei.

This method switches the roles of the projectile and the target, presupposing a beam made up of elements representative of the human body and a target composed of protons; in this way it is possible to have fragments with almost the same velocity of the incident beam and a detectable range. In order to have an enriched proton target, while avoiding managing a pure Hydrogen one, FOOT has implemented a double target made of carbon and polyethylene, respectively, from which the fragmentation cross section, on protons, is obtained through subtraction.

The employment of the inverse kinematics and the use of a double target requires a high precision level on measurements.

A relevant part of this thesis is represented by the analysis of simulated data of nuclear interactions and by the consecutive evaluation of the kinematics distributions, in direct and inverse kinematics, of the produced fragments.

This thesis, in Chapter 1, will expose the biological and physical aspects of hadrontherapy including a comparison with radiotherapy.

Chapter 2 will present the FOOT experiment thoroughly: all the detectors will be shown with their design, material and function. The expected goals and the experimental requirements of the experiment will also be underlined.

Chapter 3 will deepen the Inverse Kinematics approach knowledge introducing the process of nuclear fragmentation, explaining the roles of the projectile and target and presenting the mathematical formulation behind the method. In conclusion, some simulated plots representing the kinetic energy distribution of the expected produced fragments will be shown in order to effectively display the advantages of this experimental technique.

Chapter 1

Ionizing radiations in medical treatments

Cancer is one of the major widespread health problems and a leading cause of death worldwide. Different techniques were developed over the years in the search for a valid way to fight this enduring disease. Among the different options to contrast cancer, surgery is the standard choice of treatment in trying to remove or reduce the solid tumor. Other methods that can act as a support treatment to surgical operation are chemotherapy, immunotherapy, radiotherapy and hadrontherapy.

This thesis and, in particular, this first chapter, will focus on the understanding of the oncological side of the last two mentioned therapies and on the effects arising from radiation exposure.

The Section 1.1 will cover the biological side of radiotherapy and hadrontherapy, the damages caused to the DNA and the quantities relevant in the evaluation of effects induced on the human tissues. Section 1.2, on the other hand, will deepen the understanding of the physical aspects of the interaction of radiations with matter.

In Section 1.3 radio and hadrontherapy will be presented and confronted with the aim of underlining the advantages and disadvantages of one over the other. Section 1.4, in conclusion, will introduce the fundamental problem of the current state of hadrontherapy: the use of a fixed RBE value.

1.1 Biological effects of Radiation

1.1.1 Radiation induced damage

Radiotherapy and hadrontherapy are medical procedures that consist in radiating cancerous tissues with the goal of killing malignant tumor cells making impossible for them to reproduce, “reproductive death”. In order to avoid this cell proliferation, radiations are used to target the DNA inside the cellular nucleus. In fact, a radiation crossing an organic tissue damages the cell molecules by interacting with the matter and causing the ionization of its atoms. Therefore, they start ejecting electrons that initiate a cascade of ionizations as they collide with other molecules. These electrons can also induce chemical interactions, which may break the chemical bonds, leading to major functional and/or structural damages to the DNA. Moreover, when the incident radiation is constituted of heavy particles, secondary ionization is usual.

The majority of lesions, usually, are successfully repaired, but, in some cases, a permanent damage can occur and be lethal for the cell. Furthermore, sometimes, late reactions can take place damaging healthy cells and leading to the formation of secondary tumours. Therefore, the key problem, in this kind of therapy, is to deliver the dose in such a way that the planned target

volume receives the totality of the needed dose while sparing surrounding tissues. The damage caused by radiation can be of two kinds: direct or indirect. In the first case, the DNA is directly ionized by the incoming radiation and the double helix, that constitutes the DNA, is affected by it and a strand break is induced. Many structural alterations can happen, but the two most probable are SSB (Single Strand Breaks) and DSB (Double Strand Breaks) [2]. Their effect is shown in Figure 1.1.



Figure 1.1: Graphic representation of a Single Strand Break (on the left) and of a Double Strand Break (on the right).

The SSB (Single Strand Break) takes place when only one chain is damaged, while the other remains unaffected. It is easy to repair because the spoiled piece is removed and replaced based on the information carried by the complementary chain. On the other hand, the DSBs (Double Strand Breaks) are more likely to happen when heavy ions interact with matter, because ionized electrons, created in this process, have a mean free path of the order of few nanometers providing a high probability of ionizing the DNA opposite strands. They cause permanent damage to the DNA because both chains are broken on the same spot and it is not possible to retrieve the genetic information. This means that heavy ions have a higher damage capability than photons, which, instead, are involved in the SSB (Fig. 1.2).

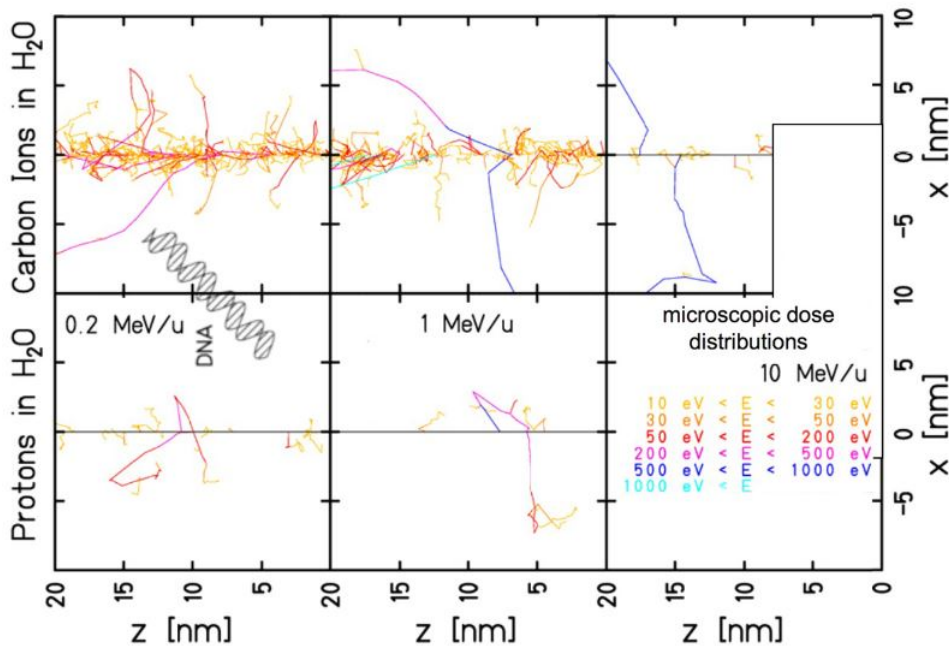


Figure 1.2: Simulation with the Montecarlo Code of the interaction between carbon ions and protons with matter in proximity of the range end, where particles slow down and their energy is of few MeV per nucleon. The graph shows the tracks of single secondary electrons. Carbon ions produce more tracks than protons, increasing the probability of having direct damage to the DNA.

The second type of damage occurs when the radiation has an indirect effect on molecules. In this process, radiolysis takes place inducing the production of free radicals, highly reactive molecules with a free orbital electron. They are created by the dissociation of water due to the incident ionizing radiation breaking the chemical bonds of molecules and leaving them with an odd unpaired electron. These free radicals interact with nearby molecules causing spread damage that can reach the DNA. Since there is a high concentration of water in the human body, the development of radicals is a non-negligible process [3].

1.1.2 Absorbed Dose

Every physical or biological effect induced in the tissue is a consequence of the energy deposited in the matter by radiation, thus the most important physical quantity in radiotherapy is the *absorbed dose*. It is defined as the mean energy E deposited by the ionizing radiation in a mass element dm :

$$D = \frac{dE}{dm} \quad (1.1)$$

It is measured in *Gray* [1 Gy = 1 J/Kg]. The absorbed dose is proportional to the energy deposited in the tissue crossed by radiation, but in case of organic tissues, it is not related to the effective biological damage. For example, a dose of 1 Gy released by a photon beam, causes a biological damage that is a lot lower than that due to the same dose released by a beam of particles with a higher charge.

1.1.3 Linear Energy Transfer

A similar related quantity is the *Linear Energy Transfer*, LET, which refers to the energy deposited by a ionizing particle, for unit distance dx , along the particle path and it is measured in keV/ μm :

$$LET = \frac{dE}{dx} \quad (1.2)$$

It is important to note that LET is inversely proportional to the squared velocity, $dE/dx \sim 1/v^2$ (see the Bethe-Bloch equation, Section 1.2.1.1, Formula 1.5)). Therefore, it has not a constant value because depends on charge, it increases with it, and, as said, it is related to the velocity of the radiation. The LET shows also a dependence on depth.

When evaluating the LET, only the energy released by primary particles is considered, while other emissions, that are far from the beam trajectory and caused by secondary particles, are neglected. In order to do that, it is possible to impose an upper threshold, Δ , for the energy of secondary electrons in order to consider only the energy deposited locally, hence excluding the interactions that carry energy far away from the original track. So, for example, Bremsstrahlung photon's deposits or highly energetic δ rays are ignored.

This physical quantity is the first step to evaluate the biological damage. In fact, since the LET value is proportional to the energy transferred by the radiation, it is directly related to the ionization density and, therefore, to biological effects. Heavy charged particles have high LET and produce clustered lesions because of their higher energy deposition density along the track path; in particular, protons with an energy of 2 MeV, have a LET of 16 keV/ μm and Helium at 5 MeV has a LET of 100 keV/ μm . Photons are considered, instead, as low LET radiations due to their sparse ionization, leading to a lower biological effectiveness. They show a LET value of 3 keV/ μm when X rays have an energy of 200 keV and a LET of 0.3 keV/ μm with a beam of 3 MeV. Technically, photons do not have a LET, hence the LET of secondary electrons, created by photoelectric, Compton Effect or pair production is associated with them.

It is important to note that radiation damage is not necessarily proportional to the absorbed dose.

1.1.4 Relative Biological Effectiveness

The linear energy transfer alone is not adequate to describe all the biological effects arising from radiation exposure. Different radiations lead to different local dose densities and diverse DNA repair responses. Therefore, another parameter is necessary: the *Relative Biological Effectiveness*, RBE. This factor is used to calculate and forecast the biological damage and it is useful in comparing the effectiveness of different ionizing particles.

The RBE is defined as the ratio of a reference radiation dose (D_{ref}), that is needed to kill a given fraction of cells, to the dose of the considered radiation (D), that is necessary to kill the same fraction of cells (isoeffect). The test radiation was historically chosen to be X rays. Therefore, the RBE is formulated as:

$$RBE = \frac{D_{ref}}{D} \quad (1.3)$$

It depends on numerous parameters among which are the particle type, the dose, the energy value and the radiosensitivity of the tissue. Consequently, this parameter can change even within the tumor itself.

It has been shown that the RBE can range from 1.5 to 2.1, but there are some exceptions as for carbon which has an assumed value of about 3 and protons to which is associated a RBE value of 1.1.

RBE shows also a dependence on LET; in fact, to a higher LET corresponds a greater number of ionizations along the path inducing a more important damage and this, as mentioned before, is associated with a high RBE value.

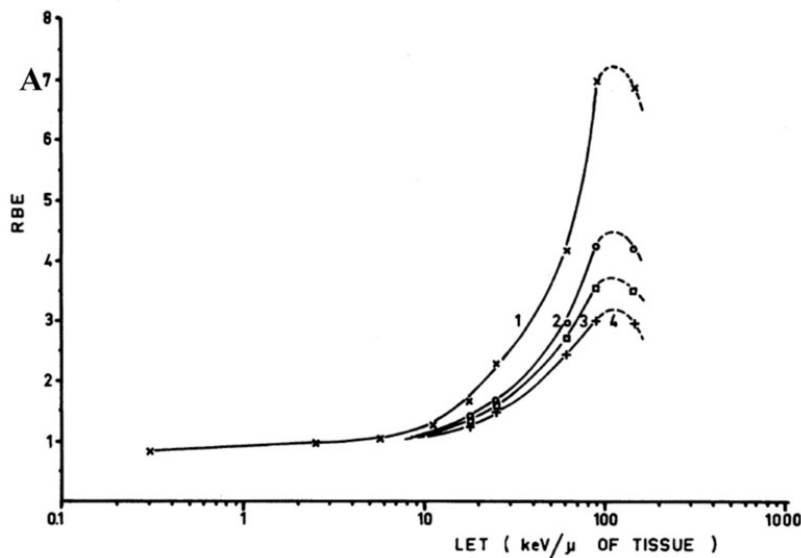


Figure 1.3: RBE as a function of linear energy transfer for human kidney T1 cells irradiated with four beams of mono-energetic alpha particles [4].

Analyzing Figure 1.3 it can be seen that the RBE increases slowly with LET up to a maximum value at about 100 keV/ μ m. The peak is caused by the *overkill effect* that happens when the dose deposited in the cell is so high that the quantity in excess does not comport any additional effect. The maximum value is optimal to produce irreparable biological damage. After this, for higher LET values, the RBE decreases because fewer particles are required to achieve the same dose and, as a consequence, the interaction probability reduces significantly.

Considering different particles (Fig. 1.4), the dependence of RBE on LET shows the maximum value shifted to higher LET for heavier particles because, for a given LET value, heavier ion are slower than lighter particles, leading to a higher ionization density and higher biological

effectiveness.

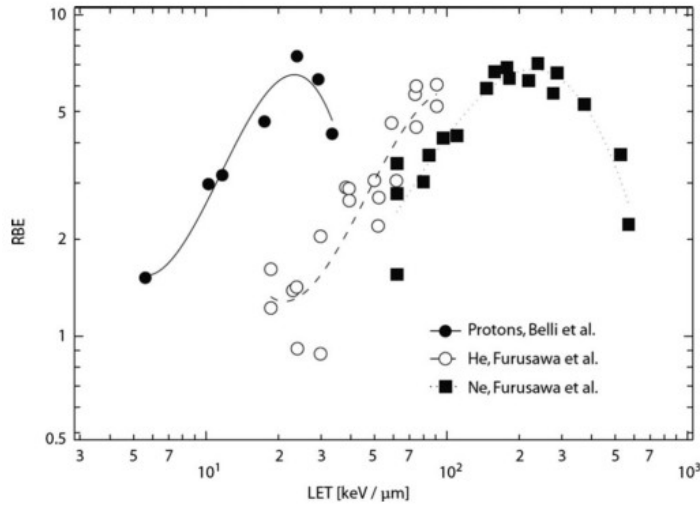


Figure 1.4: Dependence of RBE on LET and particle type.

1.1.5 Oxygen Enhancement Ratio

The presence of Oxygen in a tissue enhances the damaging effect caused by the radiation because it is a radiosensitizer and promotes the creation of free radicals. This behavior is called the *Oxygen Effect*. Therefore, an important parameter to consider in evaluating the treatment effectiveness is the oxygenation rate of the tissue. When cells have a low oxygenation rate are defined as hypoxic, meaning that they are more resistant to radiation and, hence, a higher dose is needed to destroy them. This kind of cells are usually located within the cancer because solid tumours can outgrow their blood supply, causing a low-oxygen state. The parameter that quantifies the influence of the Oxygen presence, in the efficiency of the cancer treatment, is the *Oxygen Enhancement Ratio* (OER) which is defined as follows:

$$OER = \frac{D_{hypox}}{D} \tag{1.4}$$

where D_{hypox} is the dose necessary to kill cancerous cells in hypoxic tissue and D the iso-effective dose needed to stop the cell proliferation in an oxygenated environment. Usually, the OER assumes values between 1, when the damage caused by the radiation is not influenced by oxygen, and 3, when the radiation effect is strictly related to the oxygen presence.

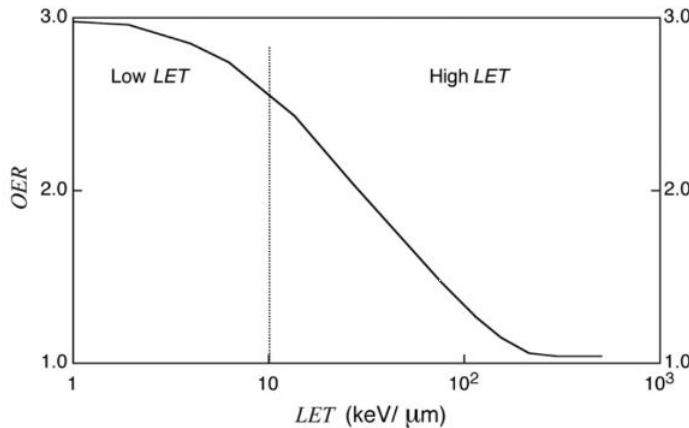


Figure 1.5: Relation between OER and RBE.

In Figure 1.5, is visible that the OER value depends on what kind of radiation is employed because it is inversely proportional to the Linear Energy Transfer. Particles with a high LET, as in the case of charged hadrons, are not influenced by oxygen levels because they have a great ionizing power and release energy in a localized way making impossible for the cells to restore. Whereas low LET radiations have a weak impact on the cells that can easily recover from the damage, therefore, the lack of oxygen negatively affects the radiation effect.

Another relation that can be pointed out is that between the RBE value and the OER. The Relative Biological Effectiveness increases with the size of the projectile ion while the OER value decreases with it as shown in Figure 1.6. For these reasons, heavy ions are good candidates for cancer treatment since they show high RBE and a low OER values.

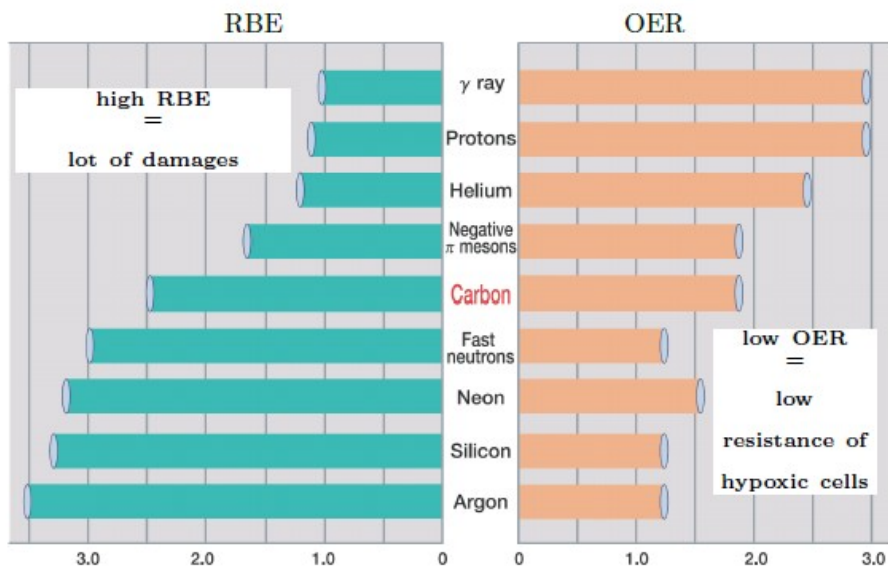


Figure 1.6: RBE (left) and OER (right) values of different particles.

1.2 Interaction of Heavy Charged Particles with Matter

Heavy charged particles are really important in this discussion because they are the central element in the therapy with hadrons. In passing through a material, they undergo two different processes: they can either lose energy or be deflected from their incident direction. Those are consequences of the collisions with the atomic electrons or are caused by the elastic scattering with the nuclei of the atoms. Between these two electromagnetic processes, the first one dominates almost entirely the loss of energy because the probability of interaction, given by the cross sections, is $\sigma_{el} = 10^{10} \sigma_{nucl}$. Another important process responsible for the particle energy loss is the nuclear fragmentation. All these processes will be explored in the next paragraphs.

1.2.1 The Bethe-Bloch formula and Stopping Power

1.2.1.1 Heavy Charged Ions

The energy loss rate is mainly ruled by inelastic collisions with target electrons. To better formulate this mechanism, it is possible to apply some approximations; for example, if the particle velocity is greater than the electron orbital velocity, the bound atomic electron can be treated as a free particle initially at rest. The momentum transfer can be assumed to be small, thus not causing the deflection of the particle trajectory and not inducing the recoiling electron to shift during the interaction. It is also necessary to neglect the particles magnetic interaction, since the electron is basically at rest. After these assumptions, the ionization process for unit of path length can be well described by the *Bethe-Bloch formula*:

$$-\frac{dE}{dx} = 2\pi N_a r_e^2 m_e c^2 \rho \frac{Z}{A} \frac{z^2}{\beta^2} \left[\ln \left(\frac{2m_e \gamma^2 v^2 W_{max}}{I^2} \right) - 2\beta^2 - \delta - 2\frac{C}{Z} \right] \quad (1.5)$$

where:

$2\pi N_a r_e^2 m_e c^2$	$\approx 0.1535 \text{ MeV cm}^2/\text{g}$
r_e^2	classical electron radius = $2.817 \cdot 10^{-13} \text{ cm}$
m_e	electron mass = 0.510998 MeV
N_a	Avogadro number = $6.022 \cdot 10^{23}$
Z	atomic number of absorbing material
A	atomic weight of absorbing material
ρ	density of absorbing material
z	charge of incident particle
β	v/c of the particle
γ	$\frac{1}{\sqrt{1-\beta^2}}$ Lorentz factor
W_{max}	maximum energy transfer in a single collision
I	mean ionization potential
δ	density correction
C	shell correction

The quantity $-\frac{dE}{dx}$ is also called *linear Stopping Power* and describes the ratio of the differential energy loss to the corresponding differential traversed thickness.

The formula 1.5 includes several correction terms due to the necessity of taking into account the quantum mechanical effects arising in dealing with light particles ($z < 10$), such as protons. A crucial term in the equation is I , the *mean ionization energy* of the material, since it rules the energy loss of the projectile and its range.

At high energies, the *density effect* correction δ arises because the electric field of the incident particle tends to polarize the atoms along its path; as a consequence, the polarization shields outer electrons from the electric field, hence, collisions with these electrons account less to the total energy loss. This factor depends on the density of the crossed material because the induced polarization is greater when the material is denser.

At low energies is the *shell effect* correction C/Z that becomes relevant; in fact, the electron in the target cannot be considered free anymore because the velocity of the incident particle is comparable or smaller than the orbital velocity of the bound electron. In the low energy region, the incident particle tends also to pick up electrons along its path, lowering its effective charge and stopping power.

However, at the energies used in hadrontherapy, the terms δ and C are negligible.

Lowering the energies even more, below ~ 10 MeV/u, z has to be replaced by an effective charge Z_{eff} because the ionization starts to interplay with the recombination process.

The energy loss rate increases as the particle slows down inside matter and reaches the maximum in correspondence of the *Bragg-Peak*, when the particle velocity is:

$$v_p \sim z^{2/3} v_0 \quad (1.6)$$

where $v_0 = e^2/\hbar$ is the Bohr velocity. For ^{12}C ions the the maximum occurs at a specific energy of 350 keV/u. Beyond this point, in the last few μm of the particle path, the energy drops to less than 10 keV/u and elastic collisions with target nuclei begin to contribute significantly to the energy loss and dominate the stopping process. This is the *Nuclear Stopping Power*.

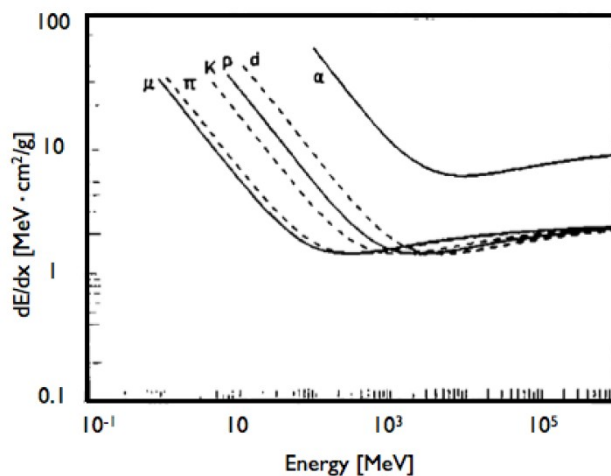


Figure 1.7: The stopping power as a function of the kinetic energy, for different particles. The minimum $\frac{dE}{dx}$ value is approximately the same for particles of same charge.

In Figure 1.7 the stopping power is plotted as a function of the particle's energy. At non-relativistic velocities, $\frac{dE}{dx}$ is dominated by the factor $1/\beta^2$, hence, it is inversely proportional to the velocity. When $v \sim 0.96c$, the stopping power reaches a minimum (similar for every charged particle); beyond this point $1/\beta^2$ becomes basically constant while $\frac{dE}{dx}$ slowly rises because of the dependence on the logarithm of the Bethe-Bloch formula. Therefore, it is shown that a charged particle, crossing a medium, loses most of its energy at low kinetic energy values and that slows down with depth. Hence, there is a greater energy release, for unit of path length, at the end of the path rather than at the beginning. This behavior, shown in Figure 1.8, is described by the characteristic function named *Bragg curve*.

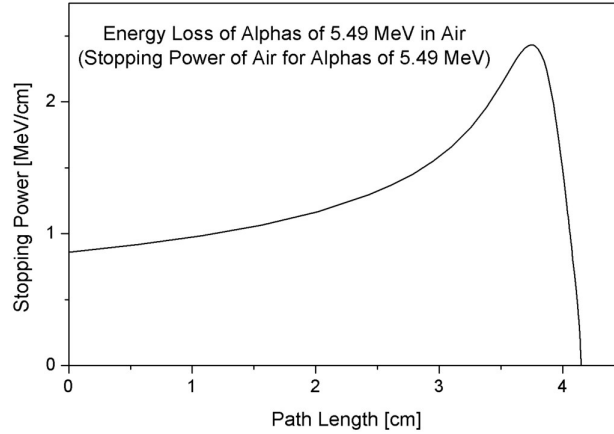


Figure 1.8: Representation of a Bragg curve.

1.2.1.2 Electrons and Positrons

When considering electrons and positrons, the Bethe-Bloch formula has to be modified because these particles interact with orbital electrons that have the same mass. The total energy loss they undergo is expressed as the sum of the loss of energy due to radiation's emission and the loss of energy due to ionization:

$$-\left(\frac{dE}{dx}\right)_{tot} = -\left(\frac{dE}{dx}\right)_{rad} - \left(\frac{dE}{dx}\right)_{ion} \quad (1.7)$$

Coulombian interaction is the main process involved in the energy loss and its contribution is expressed by the ionization term in Formula 1.7).

In addition, because of the small mass of these particles, another energy dissipation mechanism becomes relevant: *bremstrahlung*. It consists in the scattering of the particle in the nucleus electric field (radiation term in Formula 1.7); it is negligible for low energies but becomes predominant for energies of the order of some MeV. It also entails a great angular deviation that does not occur with heavy ions.

Moreover, the radiative energy loss is linear, hence, for a given energy value, it will exceed the ionization energy loss that, instead, tends to acquire a constant value. The value in which this happens is called *critic energy* E_C :

$$-\left(\frac{dE}{dx}\right)_{rad} = -\left(\frac{dE}{dx}\right)_{ion} \quad \text{when } E = E_C \quad (1.8)$$

1.2.2 Range

The path that a particle travelling through a medium covers, before losing all its kinetic energy, is an important physical quantity called *range*. It is related to the characteristics of the tissue, particle type and energy. Its accurate estimation is relevant in performing precision exposures of tumorous volumes reducing the damage to healthy tissues.

The mean range is mathematically formulated as:

$$R(E_0) = \int_0^{E_0} \left(\frac{dE}{dx}\right)^{-1} dE \quad (1.9)$$

where dE/dx is the mean rate of energy loss and E_0 is the energy of the incident particle. It is calculated in the "*Continuous Slowing Down Approximation*" that assumes that the particle follows a simplified straight path that does not take into account multiple Coulomb scattering.

This approximation is realistic and efficient for heavy charged particles since the effect of multiple scattering (Section 1.3.3) is generally small and the range corresponds to the position of the Bragg peak.

The slowing down process is not the same even for identical particles because the energy loss is affected by statistical fluctuations due to the large number of collisions. This means that the stopping point of the particle is distributed as a casual variable; this, in the case of heavy ions, generates the broadening of the Bragg peak as it is shown in Figure 1.9. Therefore, there is the effect of *range straggling*, meaning that the values spread out in a Gaussian distribution centred on the mean range (Fig.1.10).

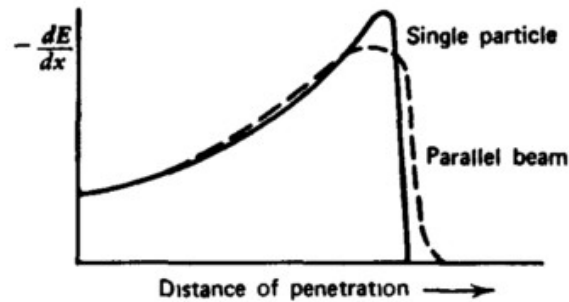


Figure 1.9: Example of Bragg curve vs penetration depth for an α particle with an initial energy of 7 MeV. Both single particle track and the average behaviour of a parallel beam of α particles of the same initial energy, are shown. The difference between the two plots is due to the straggling effect.

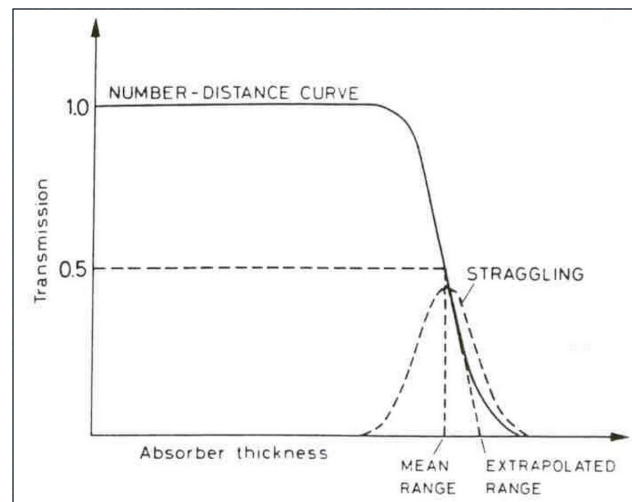


Figure 1.10: Experimental representation of the Gaussian distribution of a beam of identical particles around the mean range.

For heavy charged particles, this distribution approximation fails at large angles because is also necessary to take into account the effect of nuclear interactions that generates a tail in the distribution, behind the Bragg peak.

1.2.3 Multiple Scattering

The main process, that a charged particle crossing a medium undergoes, is the inelastic electromagnetic interaction with electrons that causes energy loss by ionization. However, the particle can also interact with the target nuclei elastically, in a process called *multiple Coulomb scattering*. It induces great angular deflections that have the overall effect of deviating the particle

from the initial beam trajectory.

In this diffusion process, the main mechanism of energy loss is that of bremsstrahlung that consists in the slowing down of the particle and the consequent emission of a photon, as depicted in Figure 1.11 .

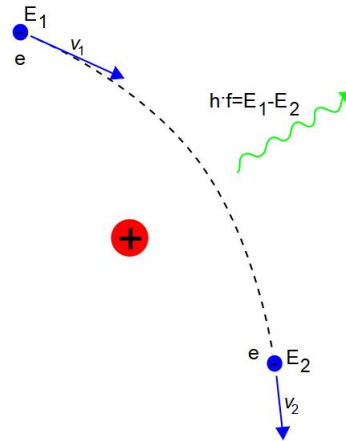


Figure 1.11: Bremsstrahlung produced by an electron deflected in the electric field of an atomic nucleus.

1.2.4 Nuclear Fragmentation

Another important phenomenon to take into account in the stopping process of high energy ions (energy of the order of hundreds of MeV), in a thick absorber, is that of nuclear interactions (Fig. 1.12).

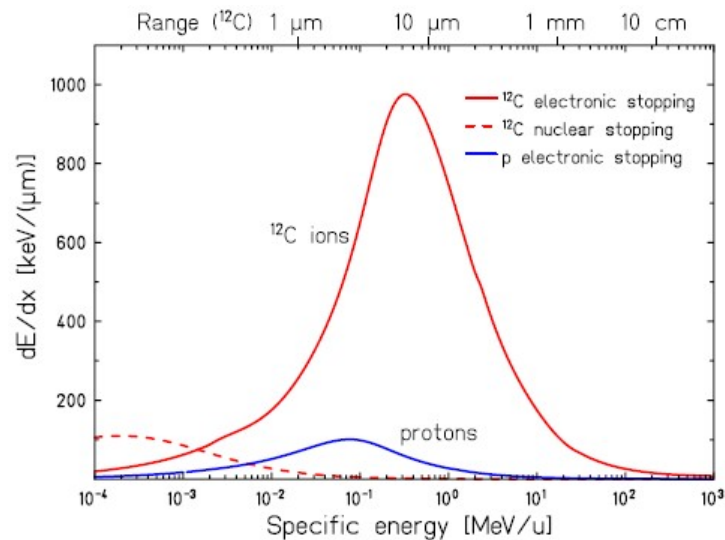


Figure 1.12: Stopping power curves for protons and ^{12}C ions in water. For protons, the inelastic collision with electrons is the dominant process for all energies. For ^{12}C ions the same process dominates almost all the dose release, except for the last few micrometers of path where the nucleus-nucleus interactions become dominant.

Although less probable than multiple scattering, nuclear interactions lead to significant effects causing the projectile or the target to fragment into lighter ions. In fact, when the energies are high enough, the projectile can overcome the coulombian barrier of target nuclei and interact directly with the nucleons.

This fragmentation process influences significantly the released dose map, generating, in case

of projectile fragmentation, the characteristic tail beyond the Bragg peak that becomes more relevant with increasing ion mass number A (Fig.1.13).

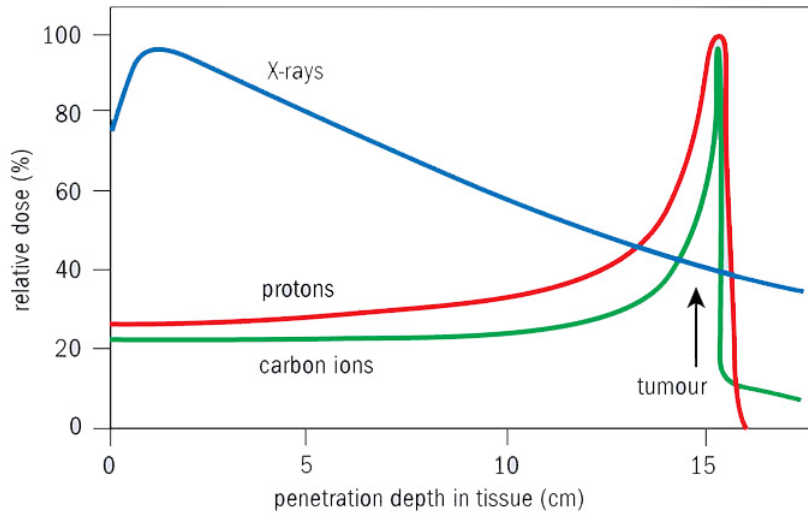


Figure 1.13: Differences in the relevance of the nuclear fragmentation process in the dose profile of protons and Carbon ions. In proton irradiation the dose beyond the peak is really small, while in Carbon irradiation there is the formation of a dose-release tail.

Nuclear interactions can be elastic or inelastic. If the incident particle undergoes an elastic interaction the kinetic energy is conserved and this leads to an angular deviation of the projectile. When, on the other hand, an inelastic collision takes place, the produced effect is more relevant because the kinetic energy is not conserved and the interaction may result in the fragmentation of the incident particle and/or of the target nuclei. Consequently, this leads to a build-up of lighter and less charged fragments that are moving at about the same speed as the beam (Fig. 1.14). The angular distribution of secondary fragments around the initial direction causes also a broadening of the lateral spreading of the deposited dose, therefore, inducing a deterioration of the longitudinal and lateral dose profile (Fig. 1.15). The impact of this effect intensifies with depth in the medium and beam energy.

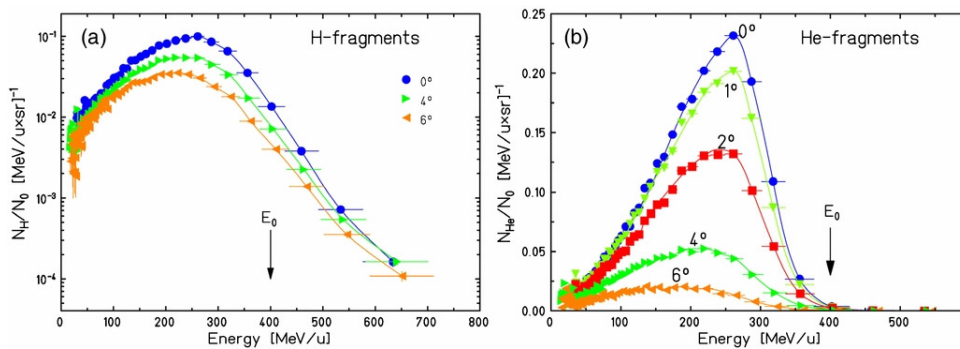


Figure 1.14: Energy spectrum of secondary particles, Hydrogen (a) and Helium (b), produced in the fragmentation of a ^{12}C beam at 400 MeV/u in a water absorber 27.9 cm deep. Distinct curves correspond to different emission angles (0° , 4° and 6° on the left and 0° , 1° , 2° , 4° , 6° on the right).

Is important to take into account the fragmentation process because, for instance, in a 40 MeV/u C ions beam on water, 70% of the primary particles do not reach the Bragg peak, undergoing nuclear reactions. A more detailed explanation of this phenomenon will be given in Chapter 3.

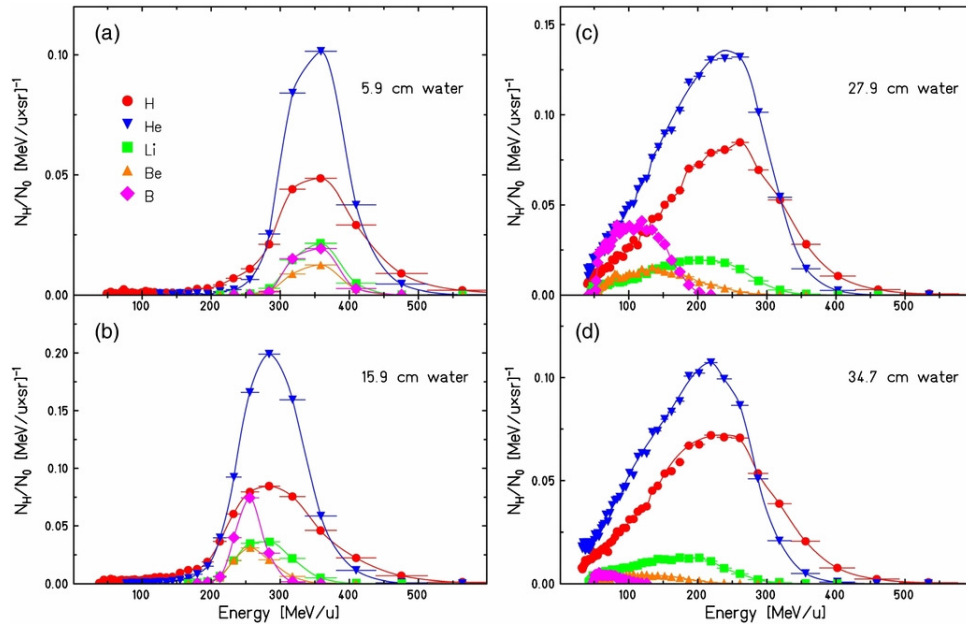


Figure 1.15: Energy spectrum of secondary particles produced in the fragmentation of a ^{12}C beam at 400 MeV/u in a water absorber. Curves correspond to an emission angle of 2° around the initial direction. Four different depth in the characteristic Bragg curve are considered: (a) entrance channel, (b) plateau region, (c) Bragg peak, (d) distal edge.

1.3 Application in Cancer Treatment

1.3.1 Radiotherapy

Radiotherapy is a type of oncological therapy that uses photon beams with energies between 6 MeV and 25 MeV and that follows an exponential law releasing energy in the patient's tissues. Its use date back to the start of the 20th century, after the discovery of X rays in 1895 by Wilhelm Röntgen.

The therapy is most often delivered in the form of photons, but a small number of treatments adopt electron beams that can be used on their own or in combination with the other therapy. Initially, X rays were mainly used but are now substituted with γ rays that are far more energetic. These photonic or electronic beams are obtained through *compact linear accelerators* (LINAC), devices that accelerate electrons to high energies through a linear tube, called waveguide, using high radio-frequency electromagnetic waves. Once reached a sufficient energy, they are shot against a metallic target that slows them down quickly and leads to the emission of high energy photons. Obtained the electromagnetic radiation, it is directed towards the patient, having acquired an appropriate direction and shape through a collimator.

The photon beam used in radiotherapy shows a characteristic depth-dose profile that follows the absorption law and, therefore, displays a steep exponential decrease of dose with depth, as shown in Figure 1.16. The release presents a maximum between 1 cm - 3 cm.

Increasing the photons' energy, the initial dose buildup, mainly caused by forward scattered Compton electrons, shifts the peak dose away from the surface of the patient's body, thereby improving the target-to-entrance dose and sparing the radiosensitive skin [5]. Moreover, the exponential decrease is less steep as the depth increases and so it is enhanced the ratio between entrance dose and target dose.

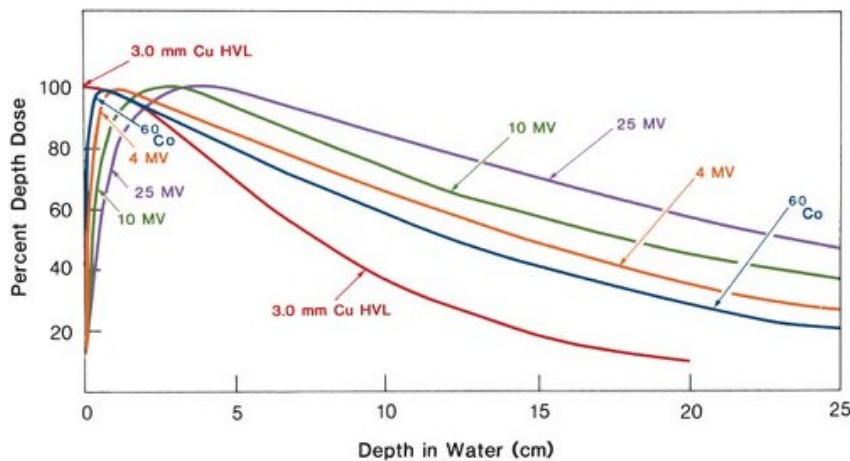


Figure 1.16: Depth dose distribution in radiotherapy for different-quality photon beams.

However, the problem arising from radiotherapy is the localization of the maximum dose release that, even at greater energies, remains near the surface of the target while tumors are often found in depth. Therefore, there is the possibility that the beam radiates mostly healthy tissues and releases a minor dose over the tumor.

Regarding biological effects, photons are low ionizing radiations with a low LET, meaning that the probability of double strands breaks (DSB) is very low and randomly distributed. As a result, this kind of therapy causes the damages to have a homogeneous distribution inside the entire radiated volume as shown in the first plot in Figure 1.17, differently from the effects arising from the employment of Carbon in hadrontherapy that are more localized.

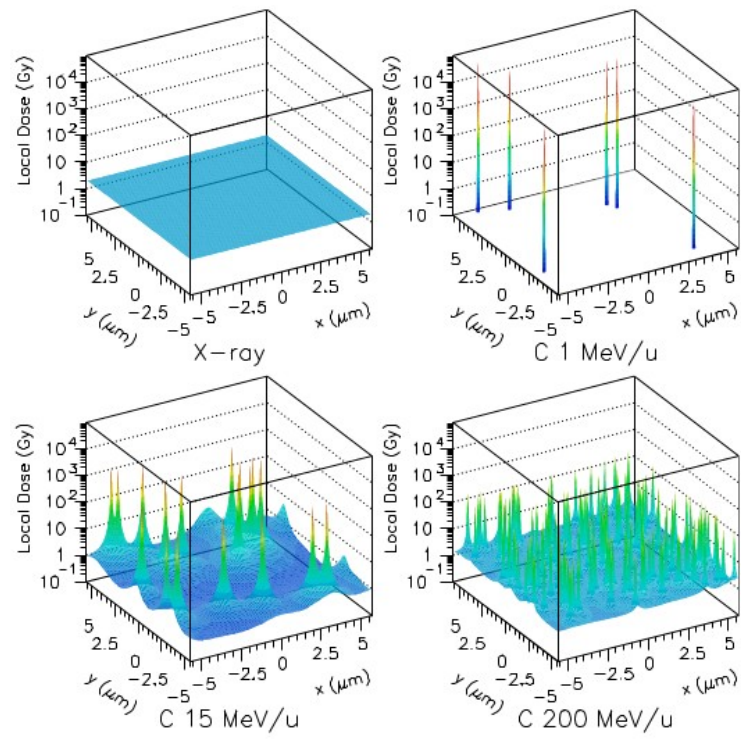


Figure 1.17: Microscopical dose distribution for different radiations. The average dose is 2 Gy.

1.3.2 Hadrontherapy

Hadrontherapy, or Particle Therapy, is an oncological technique that exploits hadrons (Greek, *hadrós*, “stout, thick”), non-elementary particles composed of quarks held together by the strong interaction. These particles are accelerated by cyclotrons or synchrotrons to energies of 60-250 MeV for protons and 100-400 MeV/u for ^{12}C ions.

It is important to underline that, at these energies, the hadrons can be seen as made up on protons and neutrons being the quark degree of freedom negligible.

Their use in medical treatments was first proposed in 1946 by Robert R. Wilson and the first patients were treated in the 1950s in nuclear physics research facilities. Initially, the clinical applications were limited to few parts of the body, as accelerators were not powerful enough to allow protons to penetrate deep into the tissues, but in the late 1970s improvements in accelerator technology, coupled with advances in medical imaging and computing, made proton therapy a viable option for routine medical applications [6].

The first hadrontherapy centre was in Loma Linda (USA), followed by the Heavy Ion Medical Accelerator (HIMAC), at the National Institute of Radiological Science (NIRS) in Chiba (Japan), where treatments with carbon ions started in 1994. Since then, more and more facilities have begun using this therapy and, up to now, there are about 100 centres operating with heavy ions worldwide.

Initially, different heavy ions like He, Ar, Si, Ne were tested to improve the effectiveness of ion beam therapy but, eventually, Carbon-12 was recognized as the optimal choice. In fact, protons and ^{12}C are now the most exploited charged particles in this type of treatment that offers significant advantages in the case of deep-seated tumors, in comparison to conventional photon therapy.

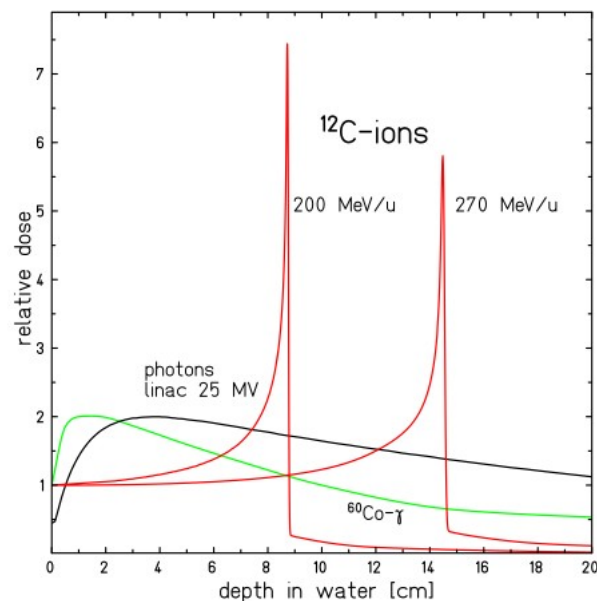


Figure 1.18: Comparison of depth-dose profiles in water of photons and high-energy carbon ions.

This therapy shows a distinctive dose release profile that makes it more effective than radiotherapy; it is characterized by a distinct narrow peak, *Bragg peak*, at the end of the particles path with a sharp fall-off at the distal edge (Fig. 1.18). The distribution shows a small entrance dose, a well-defined range and a small lateral beam spread. Charged particles follow the Bethe-Bloch formula (see Section 1.2.1.1, Formula 1.5) while losing energy per unit of path-length. This equation shows that, at the beginning, the particle loses a relatively small amount of energy in the tissues, because its velocity is high and because it has a little time to interact with the electrons of the media. Later, in the final part of the path, the kinetic energy decreases and it is possible to have a longer interaction time between the projectile and the target electrons,

resulting in a higher energy transfer and a higher energy loss just before the hadron stops. The linear energy transfer of heavy ions increases significantly towards the end of their range, thus they are biologically more effective in the peak than in the plateau region [7]. For this reason, charged particles are defined as densely ionizing radiation in contrast to photons being considered sparsely ionizing radiation [8] (Fig. 1.19).

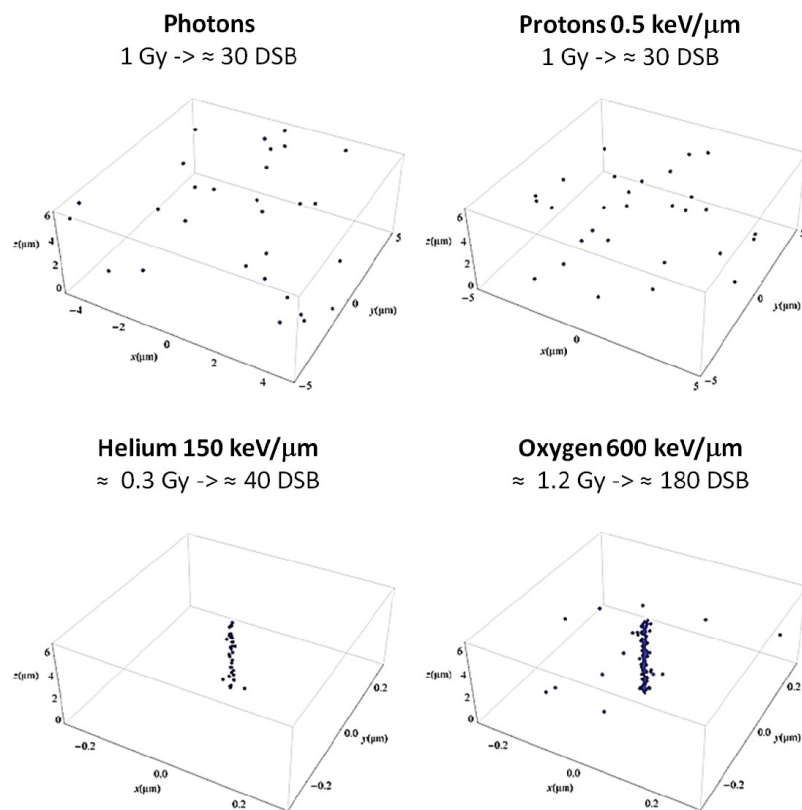


Figure 1.19: Simulated patterns of DSB distribution after photon and ion irradiation in a typical cell nucleus (radius of $\approx \mu\text{m}$). Protons are shown at the typical LET assumed in the entrance channel. Low energy alpha particles and oxygen ions show a considerable dose release in the nucleus after a single particle traversal; a high dose is released close to the particle track, resulting in the induction of an increased number of close-by DSB (densely ionizing radiation).

The peak's width depends on longitudinal and lateral energy dispersion of the beam and on the amount of matter crossed. For instance, the carbon peak is narrower than protons' one because heavier ions are less influenced by multiple scattering. In addition, the position of the peak can be adjusted to the desired depth in tissue by changing the kinetic energy of the incident ions (initial beam parameters) (Fig. 1.20 - Fig. 1.21).

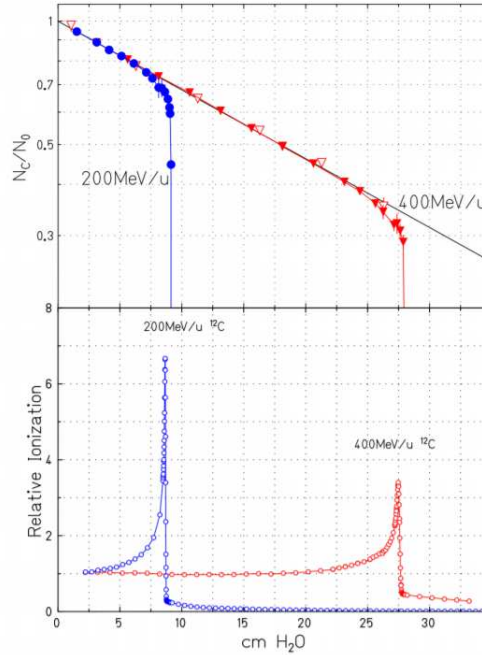


Figure 1.20: ^{12}C beams attenuation in water (upper plot) and corresponding Bragg peaks (lower plot).

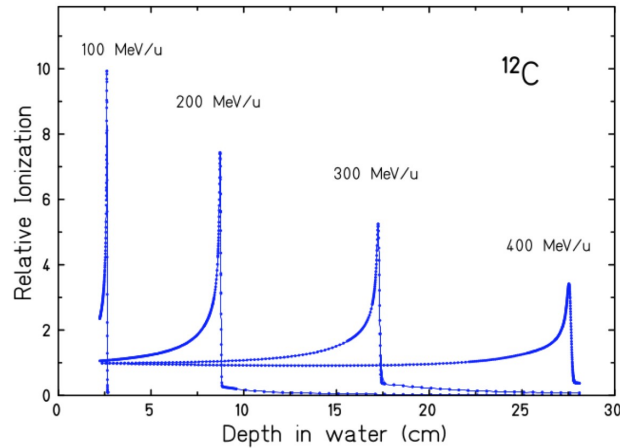


Figure 1.21: Bragg peak position for different kinetic energies.

Protons and carbon ions, despite being both employed in the therapy, have different features for what concerns the biological effects and the dose tail. Protons have a similar biological response to photons, considering the same absorbed dose, while heavy ions show higher effectiveness. In addition, heavy ions, unlike protons, exhibit a distinctive dose tail beyond the Bragg peak, caused by secondary fragments produced in nuclear reactions along the stopping path of the ions, resulting in a non-negligible amount of dose deposited in healthy tissues located beyond the tumor.

Hadrontherapy of deep-seated tumors requires ion beams with great ranges in tissue that can reach depths up to 30 cm. They need specific energies that go up to 220 MeV/u (MeV per nucleon) for protons and helium ions and up to 430 MeV/u for carbon ions.

1.3.2.1 Spread Out Bragg Peak

A custom practice, in the clinical application of hadrontherapy, is the superimposition of different ion beams with different energies, hence, various penetration distances in the patient body. It is essential since the width of the Bragg peak is too narrow to cover all the tumour volume. In order to obtain a broader irradiation profile, this technique is applied and an extended Bragg peak is achieved. It is called *Spread Out Bragg Peak* (SOBP) and it is displayed in Figure 1.22.

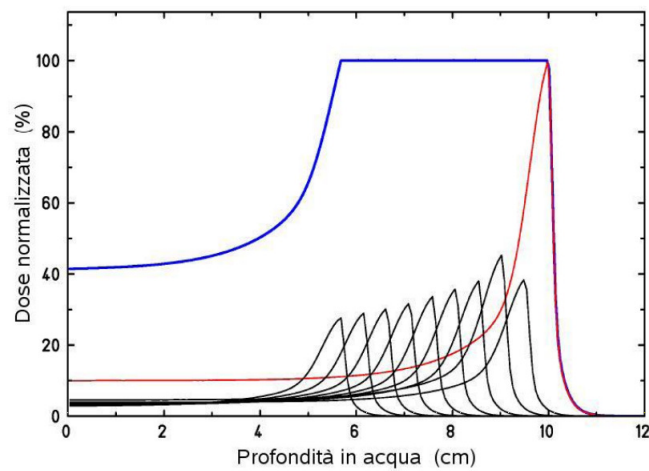


Figure 1.22: Dose profile as a function of depth for a proton mono-energetic beam (red line). From the overlapping of different energy proton beams (black lines), the SOBP is obtained (blue line).

1.4 Proton RBE

Among all the charged particles of which hadrontherapy makes use, protons are one of the most employed. Despite the fact that nowadays the proton therapy is a common technique to treat neoplastic disease, there is still a lot to study about the biological response of the tissues. Since the beginning, the dose specification in proton radiation therapy has been based upon a generic RBE, a single value that is applied to all proton beam treatments independently of dose/fraction, position in the Spread Out Bragg Peak (SOBP), initial beam energy or the particular tissue. The value was assumed to be 1.1 along all range, but it's important to consider fragmentation processes when studying proton therapy in order to develop a much more effective weighted RBE. When the incident beam interacts with the target in an inelastic-type collision, a non-negligible amount of fragments is produced outside of the planned area. They can derive from the target or from the projectile disintegration, according to the different conditions in which the fragmentation takes places (see Chapter 3, Section 3.2). Moreover, both these processes are associated with different produced fragments behaviours.

In the case of a proton beam the one to fragment is the target and the contribution due to nuclear interactions might be especially relevant in the entrance region (Fig. 1.23). Since secondary particles are expected to have high RBE values because of their small ranges, this could result in a variable RBE that can lead to an alteration in local dose deposition and an under or overestimation of RBE along the path.

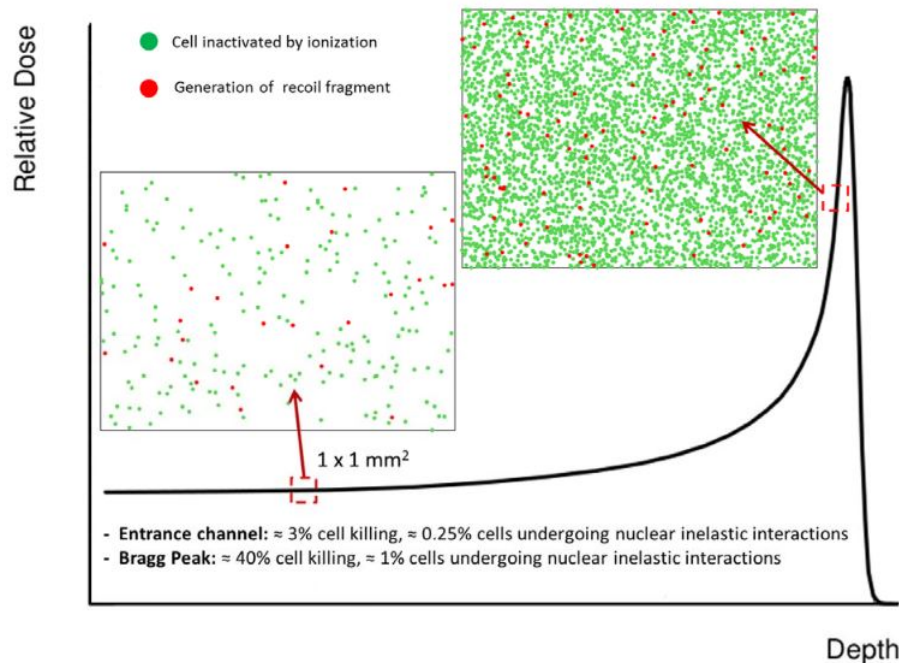


Figure 1.23: Cell killing caused by ionization or target fragmentation in tissue sections of 1 mm^2 . Red dots represent cells killed by nuclear fragments interaction, while green dots are the cells killed by electron inelastic scattering.

This is apparent in Figure 1.23 which shows that the ratio, in the entry channel, between the damage induced by fragmentation (red dots) and the one caused by ionization (green dots) is $1/8$. In correspondence of the peak, on the other hand, the ratio drastically reduces to $1/40$. Concerning heavy ions, the projectile fragments are mainly produced in the forward direction causing the delivery of harmful radiation to tissues beyond the Bragg peak (Fig. 1.24). Therefore, the fragments play an important role in spreading collateral damage to the healthy tissues crossed by the incident particles. Chapter 3 will examine in depth this collision products and it will be shown that since the fragments have higher range and different directions, they cannot be neglected in treatment planning and that is extremely important to improve knowledge of this effect in the energy range relevant for hadrontherapy.

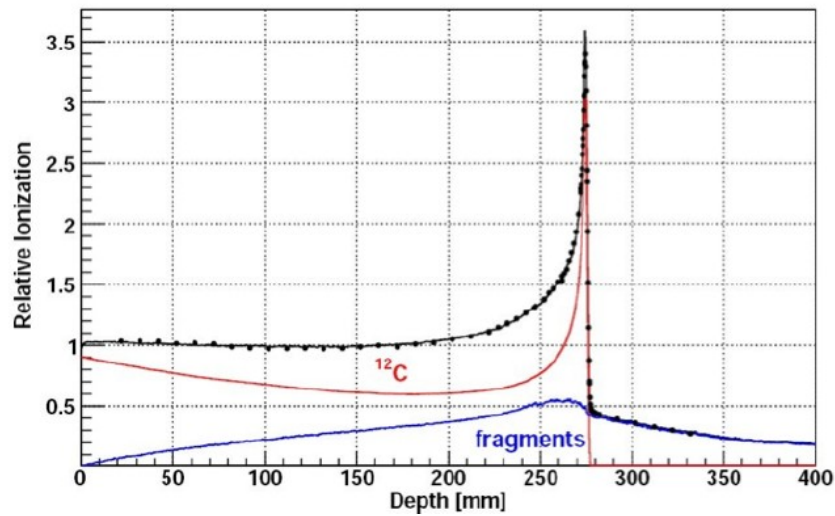


Figure 1.24: Dose release as a depth function for a ^{12}C beam at 400 MeV/u, on water. Contributions from incident beam particles (red line) and secondary fragments (black line) are shown.

The importance of a precise RBE in clinical treatment can be understood by looking at Figure 1.25: the distal end of the curve presents a delayed fall off in the case of a weighted RBE unlike with a constant RBE value. This means that neglecting the RBE variability may lead to the exposure of organs at risk (OARs) located behind the tumor. Therefore, a proper knowledge of this biological difference is very much needed.

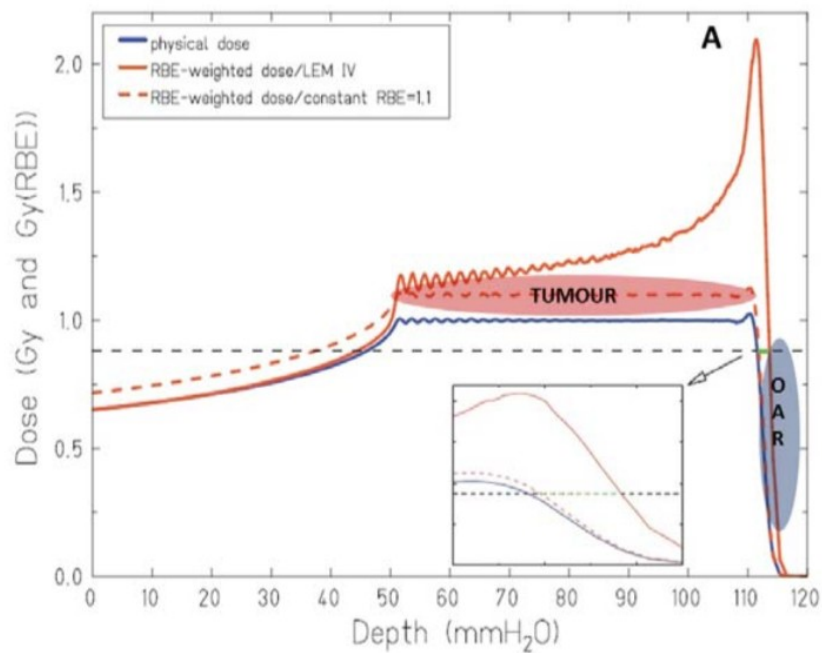


Figure 1.25: Distal fall off in the case of a weighted RBE and of a constant RBE.

Chapter 2

The FOOT Experiment

An open question in hadrontherapy concerns the lack of experimental results on the nuclear fragmentation due to the interaction of the incident beam with the human tissue. For this purpose, the FOOT (FragmentatiON Of Target) experiment was developed to measure these fragmentation cross sections. The knowledge of these data will help provide a better understanding of nuclear interactions between the beam and the patient tissues during the therapy and will enhance the accuracy of the treatment plan thanks to the calculations of the fragments distributions obtained from cross sections. In fact, the target fragmentation generates a spectrum of low energy, heavy fragments that are one of the causes behind the variability of proton RBE (see Section 1.4).

The FOOT experiment is a project supported by INFN and implemented with the collaboration of the Italian laboratories of CNAO (National Centre of Oncological Hadrontherapy), sited in Pavia, and TIFPA (Trento Institute for Fundamentals Physics Applications), along with other international institutions like the GSI (Gesellschaft für Schwerionenforschung) center and HIT (Heidelberg Ion-Beam Therapy Center) in Germany.

The data taking will take place using beams of protons, Carbon and Oxygen in the 150-400 MeV/u energy range and with the appropriate resolution for the hadrontherapy treatment. To this end, possible candidate sites for the experimental application, equipped with beams that satisfy the mentioned requirements, are the experimental halls of CNAO, HIT, GSI and TIPFA (for the calibration phase).

The need to fit the space limitations set by the different experimental and treatment rooms, has shaped the design of the apparatus that has to be easily movable - *table top setup* – and must have a length of about 2 m along the beam line while still covering the fragments angular spread.

Test beam data taking have been performed since 2017, while physical runs are foreseen for the end of 2020 and for all 2021.

This Chapter will cover, in Section 2.1, the purposes of the FOOT experiment concerning the influence of the target fragmentation in the RBE evaluation, the fragmentation of Carbon, Oxygen and Helium beams and the possibility of employing the experimental setup to gain data useful for the radioprotection in space missions. Moving on, section 2.2 will provide a detailed description of the experimental setup focusing on the two different setups implemented for the detection of heavy charged particles (electronic setup) and light fragments (emulsion spectrometer). In section 2.3 will be listed the goals set for FOOT and the experimental requirements. Moreover, section 2.4 will conclude showing the measurements that are required for the fragments identification.

2.1 The aim of the experiment

2.1.1 Target fragmentation and RBE variability

The FOOT experiment was proposed to fix the lack of measurements of the nuclear cross section data for the production of heavy recoils after proton and Carbon irradiation in the energy range of interest, up to 250 MeV and 400 MeV/u, respectively.

At the moment, the biological effectiveness does not take into account all the possible nuclear interactions between the beam ions and the nuclei of the human body that can cause various side effects.

This study of nuclear fragments spectra has a great importance in the search for accurate treatment planning systems (TPS) that aim at accounting as much as possible the biological effects arising from the fragments irradiation of tissues. The goal is to obtain a highly accurate description of the relative biological effectiveness (RBE-weighted) to supply the adequate dose. Other experiments have directed their research towards the study of projectile fragmentation, due to nuclear interaction, for different types of ions and, in particular, for ^{12}C , but the energy range addressed is still narrow [9,10]. In addition, until now, the process of target fragmentation has been almost completely neglected despite its importance, hence, the challenge will be the characterization of target fragment production cross sections for proton beams.

FOOT will also provide data for the fragmentation of high LET ions like Carbon, Oxygen and Helium beams.

2.1.2 Projectile fragmentation for Carbon beams

Carbon nuclei have an important role in cancer therapy motivated by their therapeutic advantages over proton beams as a very precise high LET radiation [11].

The knowledge of their fragmentation in the interaction with the human body is important to evaluate the spatial profile of the deposited dose and the damage to the tissues neighbouring the tumour.

2.1.3 Projectile fragmentation for Oxygen beams

In the last chapter was underlined the importance of the presence of Oxygen in cancerous tissue in promoting the biological effectiveness of radiations. To this end, Oxygen beams have started being considered as an effective tool against hypoxic tumours [12]. They are selected for their features similar to those of Carbon ions, but, most importantly, for their high LET value that, as already established, is associated with a low OER. However, in normal conditions, these beams show a larger fragmentation in the target and entrance channel, making their use less convenient as compared to lighter ions, such as C, producing a worse peak-to-entrance ratio.

2.1.4 Projectile fragmentation for Helium beams

The FOOT experiment will also focus its attention on Helium beams because they seem to be a promising alternative to protons and higher LET ions [13]. The advantage of introducing Helium ions over protons consists in the lower impact of multiple Coulomb scattering that allows a higher resolution in close lateral proximity of organs at risk (Fig. 2.1) [14]. Moreover, compared to Carbon ions, these beams have a much lower impact of nuclear fragmentation in critical regions like the tail after the peak. In conclusion, Helium has an increased biological effectiveness in the target and a more affordable implementation cost that makes it an optimal candidate for medical therapy.

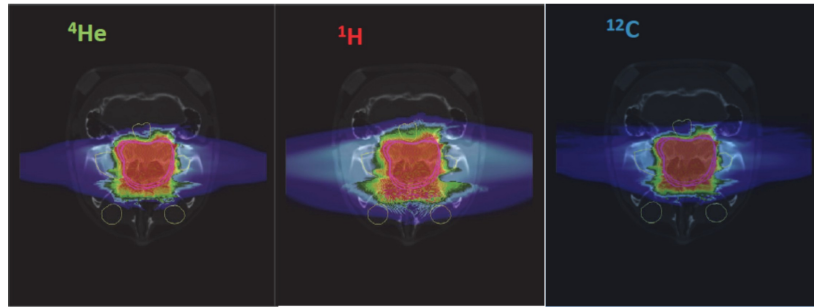


Figure 2.1: Comparison of treatment plans, on a skull cancer, showing the little lateral diffusion of Helium ions, much more convenient as compared to protons and Carbon ions.

2.1.5 Radioprotection in Space

The measurements performed by FOOT are not only suitable for therapeutic purposes but for other applications too, like radioprotection in space [15]. With the same experimental method it is possible to assess the risk for astronauts in perspective of long duration space missions for what concerns the radiation sources that can be found in space. It is important to quantify the radiation field within the vessel and, thus, the cumulative dose received by the human inside. However, knowing accurately the composition and energy spectrum of space radiation particles is not sufficient because the radiation outside the spacecraft is modified by the interaction with its walls and its shielding material. Therefore, atomic and nuclear interactions occurring between the incoming particles and the material of the vessel need to be characterized. With fragmentation process data is possible to design and optimize the spacecraft shielding in order to consider lighter fragments with a higher penetrating power. This study is really important because some of these radiations have the capacity of inflicting a lethal dose to the astronauts as in the case of protons emitted from the sun during coronal mass ejections and solar flares (SPEs – Solar Particle Events). Other harms could arrive from Galactic Cosmic Rays (GCR) and geomagnetically trapped particles that are considered to be among the most significant hazards for humans in space. Typical energies are of the order of GeV and can be measured by FOOT.

Despite the differences, there is a common ground between pursuing radioprotection against the harmful effects of space radiation and providing tumor therapy to patients using ions. In fact, the particle species of interest to medical therapy, such as protons, Carbon ions, Helium and Oxygen are among the most abundant in space, as well. In addition, the energy range for tumor therapy is not far from the typical energies of space particles that, on average, can reach values in the GeV range. In addition, as in the case of therapy-oriented analysis, measurements on hydrogen targets will be required also for radioprotection, because hydrogen-rich materials are among the best shielding options. Therefore, these shared interests allow the interchange of cross sections data. FOOT will carry out measurements of the fragmentation cross section of H, ^4He and ^{12}C beams with kinetic energy extended up to 1 GeV/u with the main focus of Z identification.

2.2 The experimental setup

The design of the setup is driven by the necessity of detecting very short range (order of tens of microns) and very low energy (few MeV) fragments produced by the target fragmentation due to the interaction with the proton beam. It is necessary to take advantage of an inverse kinematics approach that switches the roles of projectile and target in order to have secondary fragments with boosted velocity and a dose deposition outside the planned target region. Therefore, FOOT will study the fragmentation of different ions beams (C, O, ...) onto hydrogen-enriched target where secondary fragments have more energy and a much longer range, making their detection easier. Chapter 3 will focus entirely on this fundamental technique.

Another major point to take into consideration when designing the apparatus, it is that the setup has to be built so that is assured a good balance between the production cost, the portability and the necessity for the largest possible geometrical acceptance for the fragments. The setup will analyze the produced fragments and obtain their trajectory, momentum, kinetic energy, Time Of Flight (TOF) and $\frac{dE}{dx}$.

The first region that the incident beam encounters, in its path inside the apparatus, is represented by the upstream region. This has an important role in the experiment because provides a counter for the rate of the ion beam, the trigger signal to start the TOF measurement and a track of the beam position and direction. All these data are fundamental for the application of the inverse kinematics that uses the *Lorentz transformation* in order to switch back, mathematically speaking, projectile and target that, otherwise, are inverted in the actual setup.

2.2.1 Start Counter

The Start Counter (SC) is a plastic scintillator detector consisting of a 250 μm thick disk, with a radius of 26 mm sufficient to cover the typical beam transverse size. A scintillator is a material that, when excited by an ionizing radiation, absorbs its energy and re-emits it in the form of light. This produced light is then collected by 160 optical fibers grouped in four bundles and readout by four fast photomultipliers (Fig. 2.2).

The thickness of the scintillator was selected in order to reduce the pre-target particle interaction probability that has to be lower than the on-target one.

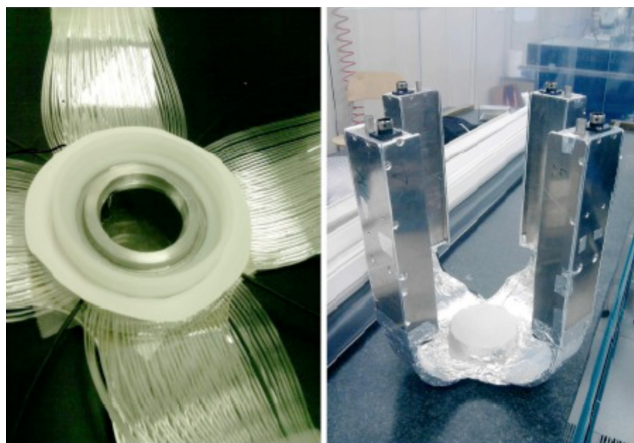


Figure 2.2: Details of the Start Counter: the scintillator and the optical fibers grouped in four arms.

The Start Counter is placed about 30 cm upstream of the target and measures the incoming ion flux necessary in the cross section calculation. This first setup element has also the function to start the trigger signal to the whole experiment giving the reference time for all the other detectors and allowing the TOF measurement in combination with the $\frac{dE}{dx}$ -TOF scintillator

detector. In the case of Carbon ions at 400 MeV/u, it is possible to reach a time resolution of 70 ps.

2.2.2 Beam Monitor

The Beam Monitor (BM) is a drift chamber detector employed to measure the space coordinates of the trajectory of a charged particle (Fig. 2.4). The detection of the particle signal can be divided in three stages.

The first mechanism that takes place is the ionization process during which charged particles ionize the gas colliding with one of the atoms and producing an electron-ion pair. Particles crossing matter lose energy following the Bethe-Bloch theory and can be detected analyzing the homogeneously distributed ionization clusters that they leave behind. It is possible for extracted electrons to cause secondary ionizations that induce a signal in the drift chamber and leads to background events.

The second stage of the particle tracking is the transport phase. The electron-ion pairs, previously generated, are subjected to the effect of an electric field and of thermal diffusion that cause the migration of pairs towards the electrodes of opposite polarity. Moreover, in this process, the particles are subjected to multiple collisions with the gas molecules. It is possible to define a macroscopic average velocity, *drift velocity*, which characterizes such migration processes. In case of a constant electric field, the inelastic collisions randomize the particles trajectory leading to a constant velocity that allows to track down the position of initial ionization exploiting the drift time interval.

The last process is the multiplication cascade that starts when the electrons approach the electrodes. The strong electric field increases their velocity and induces a great amount of ionizations that generates an "avalanche". This electron avalanche generates a fast current pulse that is later digitized and read. It allows to reconstruct the coordinate along the drift direction by considering the time difference with respect to a trigger signal.

The drift chamber employed in the FOOT experiment is composed of twelve layers of wires oriented along the x and y axes in an alternated way with the purpose of reconstructing the primary beam profile (direction and position) (Fig. 2.3). Moreover, each layer has three drift cells rectangular-shaped (16 mm x 10 mm) with the long side orthogonal to the beam (highlighted in red in the Figure). In each view, two consecutive layers are staggered by half a cell to solve left-right ambiguities in track reconstruction.

Two mylar windows, 100 μm thick, are located in front of the Beam Monitor and in correspondence of the exit region in order to contain the gas mixture of Ar/CO₂ that fills the Chamber. This setup will provide coordinates measurements of the initial beam.

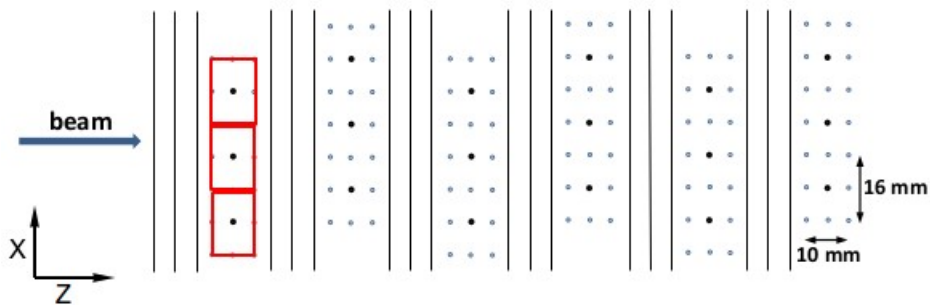


Figure 2.3: Wire placement and cell structures in the Beam Monitor (example shown on the second plane). It is possible to see the staggered layers.

The Beam Monitor will be placed between the Start Counter and the target and will measure the direction and impinging point of the ion beam on the target. It is important to know where the beam has encountered the target because it helps resolving the pile-up ambiguity that can

appear in the following vertex detector (VTX). In fact, if there is a good alignment between BM and VTX, the positions of the vertices reconstructed by the VTX for each event can be compared with the position of the BM track, and only the closest vertex to the BM extrapolation is selected as a matching vertex. Thanks to the fast read-out time (order of 1 s or less), compared to the VTX read-out time ($=187 \mu\text{s}$), the BM can ensure that tracks belonging to different events cannot be mixed.

Another purpose of the BM is to reject the events in which the primary beam undergoes a nuclear inelastic interaction before the target.

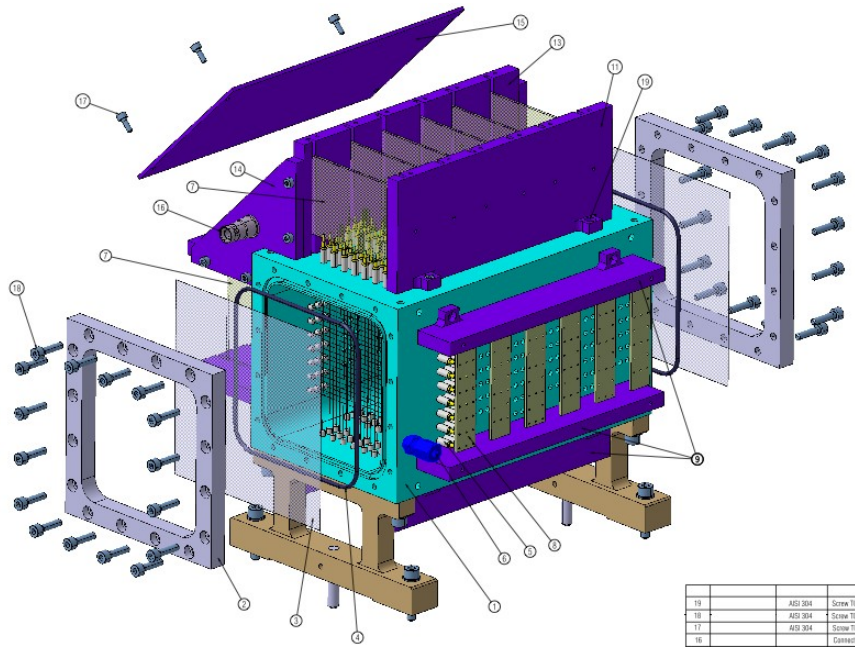


Figure 2.4: Representation of the Beam Monitor drift chamber.

2.2.3 Fragments detection setup

Studying previous nuclear fragmentation experiments and analyzing models elaborated through Montecarlo simulations it is clear that is not possible to detect all secondary fragments with an apparatus of limited size. Lower mass fragments ($Z \leq 2$), such as protons and deuterons, in fact, display a wider emission angle than that of heavier nuclei that, instead, are ejected in a forward direction. Therefore, the setup needs to be extended in order to appreciate both kind of ions; however, the necessary size and weight of an apparatus capable of doing this, would become impracticable considering the spatial limitations already mentioned. To solve this problem, the FOOT experiment will implement two different setups for the two fragments mass intervals.

Heavier fragments ($Z > 2$) will be detected with a setup covering an angular acceptance of 10° (Fig. 2.5), with respect to the beam axis, while lighter particles will be revealed with an emulsion chamber capable of extending the angular acceptance up to about 70° .

Detection of Heavy charged particles

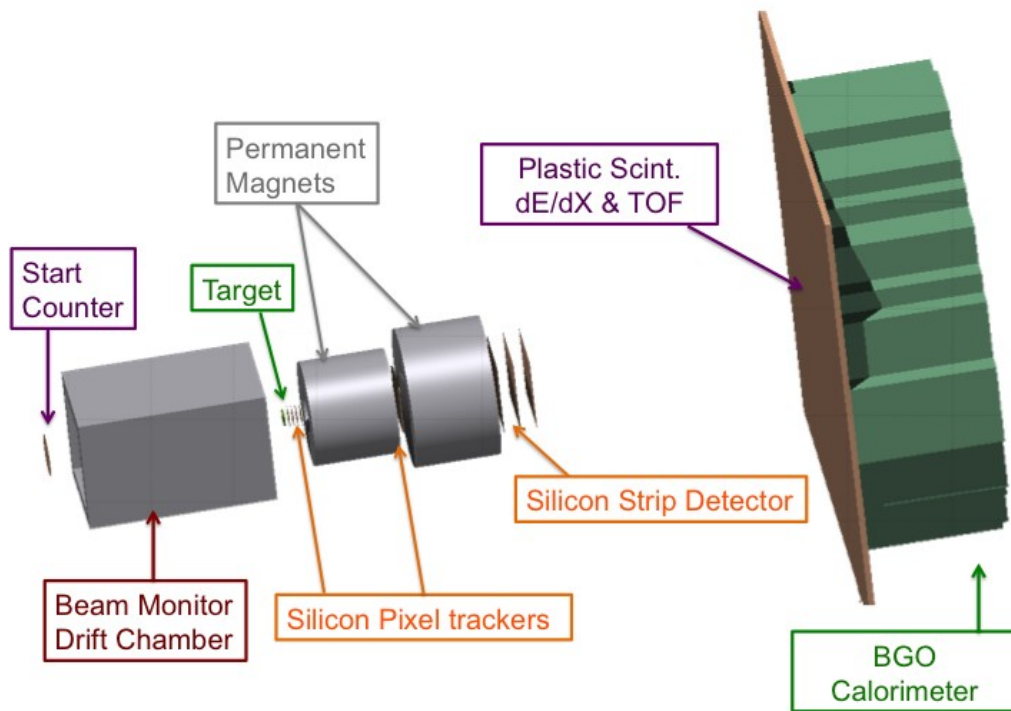


Figure 2.5: Schematic view of the FOOT apparatus for heavy particles.

2.2.3.1 Target

After the Start Counter and the Beam Monitor, the target can be found. It is composed of two layers of polyethylene C_2H_4 and carbon C, respectively, thanks to which it is possible to perform measurements of the proton cross section that is obtained from the subtraction of the two layers cross sections, as will be thoroughly discussed in Chapter 3.

The thickness of the target is chosen to be about 2 mm in order to prevent the possibility of

trapping the fragments, as would happen with a thicker target, but to also avoid the excessive drop in the interaction rate that, on the contrary, happens when employing a thin target.

2.2.3.2 Magnetic Spectrometer

The magnetic spectrometer represents the tracking system of FOOT. It is arranged in three measuring stations: two upstream stations of monolithic pixel sensors and a telescope of silicon microstrip detectors for the downstream station. In between, two permanent magnets provide the required field and perform the function of bending the fragments produced in the target.

A magnetic spectrometer is an apparatus composed of a magnet that produces a magnetic field B and one or more detectors designated to track the particle trajectory. Thanks to the *Lorentz force* ($\vec{F}_B = q\vec{v} \times \vec{B}$, where q is the charge, \vec{v} is the particle velocity and \vec{B} is the magnetic field), particles are deflected from the incident beam direction and knowing the radius of curvature (r) is possible to deduce the particles momentum. In fact, since the velocity of the beam is perpendicular to the magnetic field B , the momentum is defined as $p = rqB$.

Vertex Pixel Tracker (VTX) Immediately after the target, is placed a telescope of pixel trackers providing the vertex reconstruction and the initial tracking of the produced fragments. There are four layers of silicon detectors (Fig. 2.6) arranged in such a way that an acceptance level of about ± 40 degrees is guaranteed for the fragments produced in the target. Each sensor layer consists of a matrix composed by 928 (rows) \times 960 (columns) pixels with a side length of $20.7 \mu\text{m}$ meaning an overall size of the chip of $20.22 \text{ mm} \times 22.71 \text{ mm}$. Every sensors have a reduced thickness of $50 \mu\text{m}$ in order to minimize the multiple scattering and nucleus re-fragmentation like in the Vertex. The sensors will be arranged in two sub-stations separated by a gap of about 10 mm and will consist of two sensors each at a distance of 3 mm to one another.

This setup will ensure a reconstruction efficiency of about 95% (excluding the geometrical acceptance); the measured cluster position resolution is better than $10 \mu\text{m}$ and the vertex spatial resolution is $10 \mu\text{m}$ in the plane orthogonal to the beam direction and $60 \mu\text{m}$ along the beam direction.

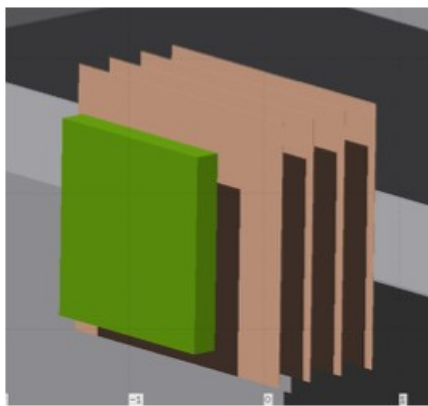


Figure 2.6: Target (green) and vertex tracker (brown) geometrical scheme.

Permanent Magnet The setup involves the use of two permanent magnets with Halbach geometry meaning that the dipolar magnetic field is obtained with magnets of cylindrical shape where the internal cylindrical hole presents a rather uniform magnetic field of 0.8 T (Fig. 2.7). The magnets are arranged to leave a central aperture of 4.5 cm in radius and are made of twelve

single pieces of SmCo (Samarium-Cobalt) or NeFeB (Neodymium-Iron-Boron) (with a width of 10 cm). It is important to choose wisely the material, dimensions and thickness of the magnets because they affect the produced field and contribute to the achievable strength. Simulations have shown that the required level of performances can be achieved with a total weight and size that is compatible with the inspiring concept of portability.

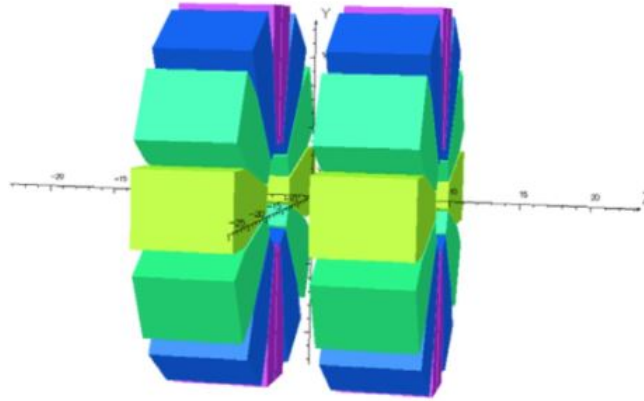


Figure 2.7: Halbach configuration for the double magnet design.

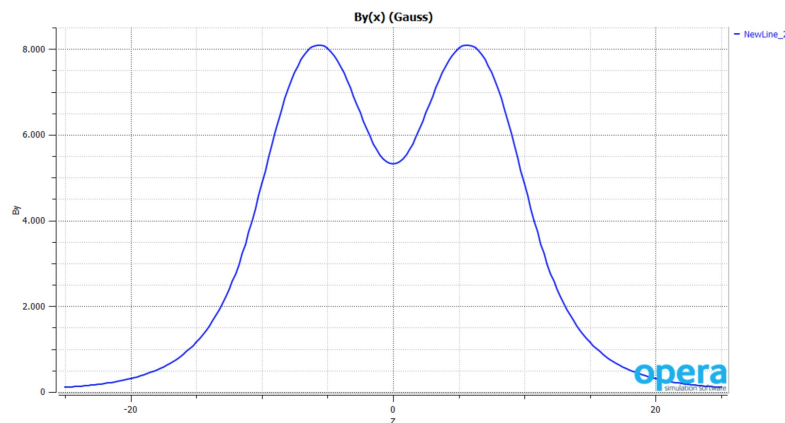


Figure 2.8: Magnetic field amplitude (Gauss) along the axis of the two magnets system. A not uniform magnetic field is approximated by the convolution of two Gaussian distributions each relative to a single magnet.

Inner Tracker Station Between the two magnets there is the second silicon pixel tracker that consists of two planes of pixel sensors to improve the trajectory and momentum measurement. Inside the two layers is placed a 2 mm thick plate of SiC (a low density foam) as a spacer. Therefore, this detector has the same structure of the VTX but covers a larger area of about 8 cm x 8 cm.

In the region occupied by the inner tracker the residual magnetic field is not negligible ($\sim 0.6\text{T}$) (Fig. 2.8) but the sensor outcomes should not be significantly affected. The only flaw is that the performances will be slightly influenced by the mechanical arrangement that needs some more material to hold the sensors, now covering a larger area, and to fix the distances between the two planes. The cost will also increase due to the need for more material.

Outer Tracker The last tracker downstream the magnetic volumes is a Microstrip Silicon Detector (MSD). It is used to perform a global tracking with the other silicon detectors and to match the reconstructed tracks with the hits in the TOF scintillator and the calorimeter. It

will also provide a redundant measurement of $\frac{dE}{dx}$ that is relevant for the improvement of the reliability of the experiment.

The Microstrip Silicon Detector covers an area of $9 \times 9 \text{ cm}^2$ according to the 10° opening angle needed to detect heavy ions. Each component microstrip is as long as the entire detector. It is a p-n junction tracking detector (*Ionization Detector*) where the electron-hole pairs, produced by the incident particle, are collected in the electrodes. This induced current generates a signal that is later amplified thanks to a Low Gain Avalanche Diode (LGAD). From the obtained signal is possible to reconstruct the fragments trajectory inside the detector.

A benefit of this kind of detector is that it requires a reduced amount of material meaning that the impact of multiple scattering and of secondary fragmentation is minimized. It is made of three x-y planes with a 2 cm gap between them, along the beam direction. Each plane has a thickness of about $150 \mu\text{m}$ obtained by two silicon planes of $70 \mu\text{m}$ glued together using a $30 \mu\text{m}$ thick bi-adhesive giving an equivalent silicon thickness of $\sim 155 \mu\text{m}$. The MSD allows to achieve stopping power measurements with high level precision, in a wide kinetic energy range, useful for hadrontherapy and radioprotection in space studies.

2.2.3.3 Identification Region

Scintillator Downstream the magnetic spectrometer region, there is a Plastic Scintillator with the task of providing the stop to the TOF measurement, began in the Start Counter, and to measure the energy release in a thin slab of plastic scintillator, $\frac{dE}{dx}$, to identify the charge of the crossing fragment.

Scintillators are detectors that exploit the light (photons) emitted by an ionized atom in the transition between an excited state and the fundamental level.

In this specific case, it is made of two orthogonal layers of 20 plastic (polystyrene) scintillator bars, each 2 cm large and 40 cm long. These dimensions are suitable to achieve a coverage of the angular distribution of the fragments 1 m far from the target. With optical glue, the scintillator bars are coupled, at both ends, to silicon photomultipliers that detect the light signal (photons), generated during ionization and collected by the rods, transforming it in an amplified electronic signal. The orthogonal arrangement is intended to identify the two-dimensional interaction position of the particle in the detector. Moreover, the spatial resolution in the two directions is given by the bar section, 20 mm, which matches the calorimeter pixel size. Each scintillator rod has a thickness of 3 mm (6 mm for the double FOOT layer) that is a compromise between the search for an improved resolution of $\frac{dE}{dx}$ and TOF and the necessity of reducing re-fragmentation.

Calorimeter The Calorimeter is positioned at a distance of about 100 cm from the target and has the task of measuring the energy of the produced fragments.

The fragments that reach the Calorimeter need to have a high enough energy to prompt a shower of photons and, therefore, to generate a proportional signal.

The chosen material is a dense crystal like BGO (bismuth germanate). The calorimeter needs to cover a circular surface with a radius of about 20 cm, dictated by the emission angle of the heavy fragments, meaning that about 350 individual BGO crystals with $2 \times 2 \text{ cm}^2$ transverse size will be used. This crystals granularity is requested to keep the events with multiple fragments impinging in one crystal below the percent level.

The overall crystal thickness is about 24 cm to allow containing fragments of the already discussed energy range.

An open question is represented by the energy not recovered after the nuclear interaction of the fragments with the calorimeter material, due to the neutrons production. Typically, these produced neutrons travel for an unpredictable length before undergoing any other interaction and have a non-zero probability to escape from the calorimeter leading to a systematic underestimation of the kinetic energy of the fragments.

Detection of Light charged particles

The study of low Z fragments requires the use of an Emulsion Spectrometer (ES) differently from the electronic setup employed for heavier particles. The apparatus will be positioned right after the Start Counter and the Beam Monitor. It takes advantage of nuclear emulsions and it is very effective in achieving the highest spatial resolution when tracking ionizing particles or short-lived particles.

In this setup, target and detector are integrated in the compact arrangement of the emulsion chamber that can provide an accurate reconstruction of the interactions occurring inside the target (Fig. 2.9). The emulsion setup requires neither power supply nor readout electronics.

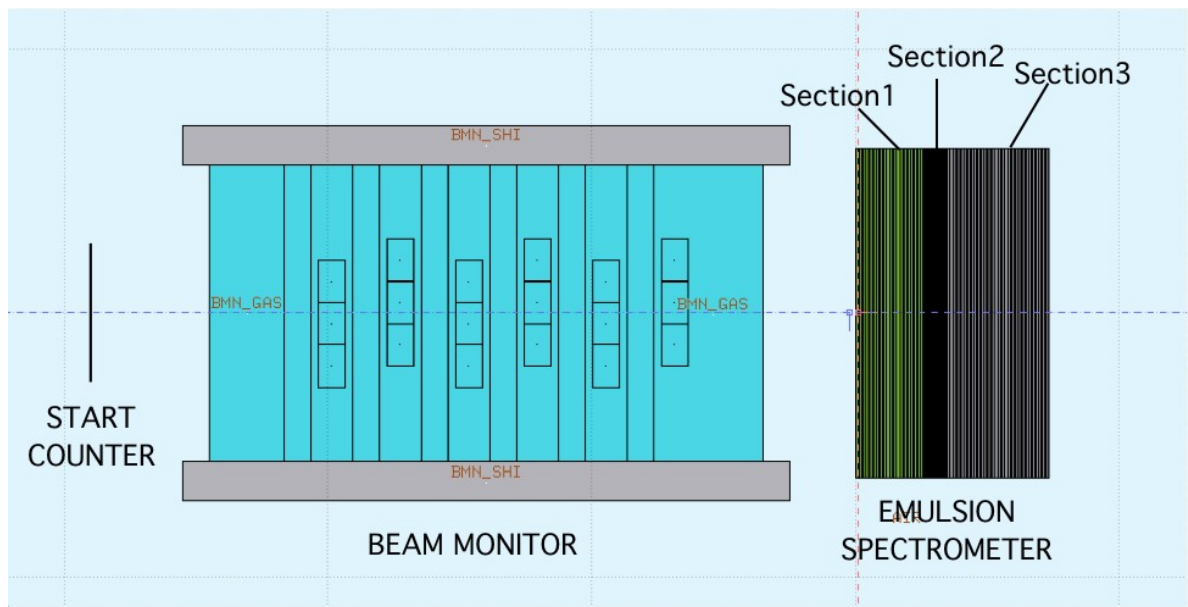


Figure 2.9: Schematic view of the FOOT apparatus for light particles.

The chamber is made of alternating passive materials, as Carbon and Lead, and nuclear emulsions films acting as both high-resolution tracking devices and ionization detectors. Each nuclear emulsion film can be divided in two sensitive layers, $50\ \mu\text{m}$ thick, that are made of AgBr (Silver bromide) crystals dispersed in a gelatin binder. These layers are then deposited on the sides of a $200\ \mu\text{m}$ plastic base, resulting in a total thickness of $300\ \mu\text{m}$. The crystals in the reactive layers record the particle trajectory and through the chemical process of development, grains are grown around the latent image centers and become visible through an optical microscope. Scanning the emulsion and then analyzing the acquired image, it is possible to associate dark pixels to the grains and to reconstruct the track of the penetrating particle recognizing clusters of aligned pixels.

Analyzing the grain density along the particle track it is possible to evaluate the fragment charge with a high efficiency (above 99%) while various elements are discerned comparing the track length of the detected particles.

The emulsion chamber will be divided in three sections (visible in Figure 2.10): vertex and tracking detector, ionization detector for charge identification and tracking detector for momentum measurements.

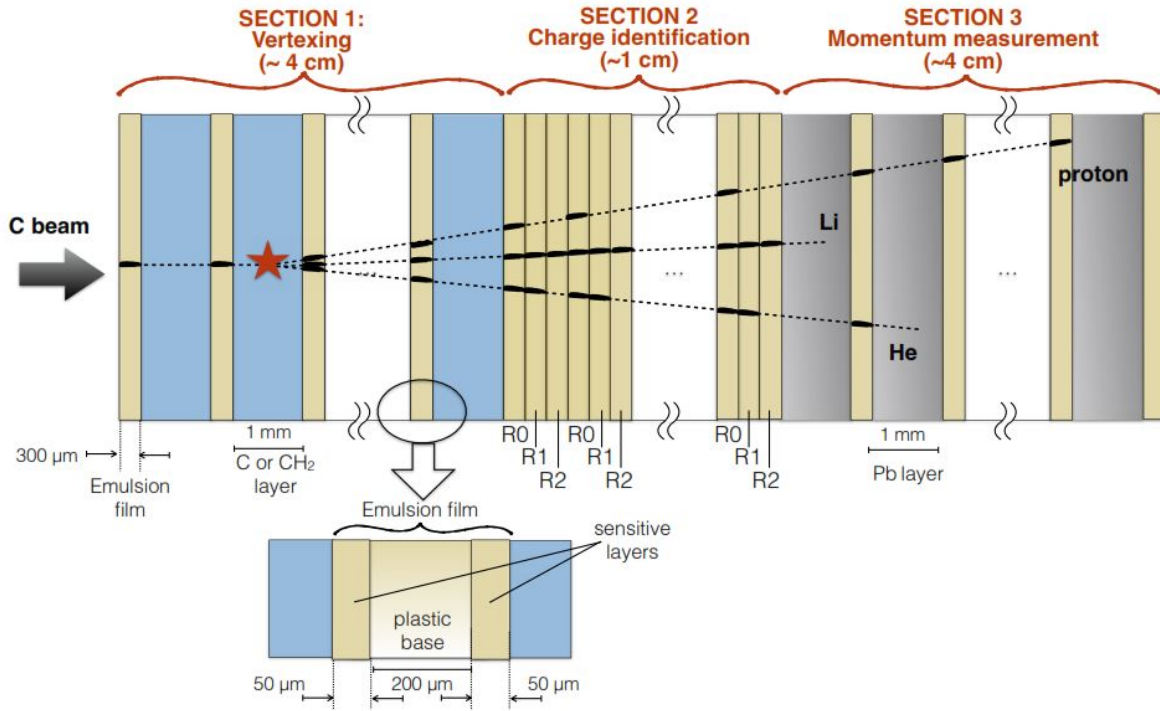


Figure 2.10: Scheme of the Emulsion Spectrometer composition.

Vertex and Tracking Detector The first section of the emulsion chamber (Fig. 2.10) will be made of Carbon or C_2H_4 layers (1 mm) cells, that work as targets, and emulsion films ($300 \mu\text{m}$) (Fig. 2.11). These layers will interact with the incident beam, originating secondary fragments that will be tracked by the detector and used to reconstruct the interaction vertex position. It is important to achieve a significant number of reactions in this section, hence, after an accurate event probability estimation, the length needed for the region has been estimated to be of 39 mm, corresponding to 60 layers.

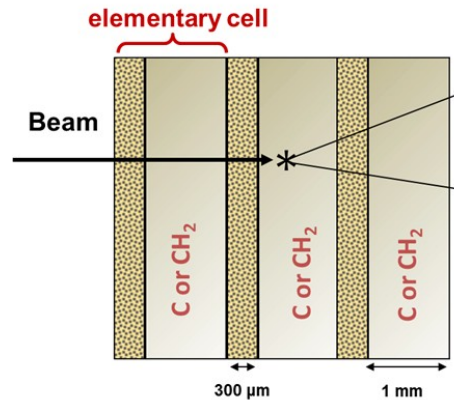


Figure 2.11: Scheme of the Vertex and Tracking detector.

Ionization Detector for charge identification The second section is designated for particles charge identification (Fig. 2.10); this can be achieved through the combination of films only, which are properly treated with different refreshing procedure after exposure. This portion of the Emulsion Chamber will be composed of several elementary cells, each containing three emulsion films.

Particles passing through a nuclear emulsion leave a trajectory, proportional to the energy loss over a certain range, which is observed as a thin track due to the specific ionization. This track is proportional to the grain density and the sum of the grain pixels belonging to the same track, normalized to a given track length, is a variable - *track volume* - sensitive to the specific ionization, hence to the particle charge. To highlight these tracks, three different treatments need to be applied to the film triplets denoted as R0, R1 and R2. They are treated at different temperatures and relative humidity after the radiation exposure and then they are chemically developed in such a way that every film shows some peculiarities. This way, after every process, a track is characterized by three volume variables, referred to as VR0, VR1 and VR2. Looking at the correlations between appropriate pairs of variables, it is possible to distinguish different particles and properly identify the fragments.

Tracking Detector for momentum measurement The last section of the emulsion chamber is designed for the momentum measurements. It consists of emulsion films alternated with 1 mm thick lead plates used as passive material (Fig. 2.12). The number of lead plates could vary, ranging between 10 and 50, with the section length that has to be set accordingly to the incident beam energy.

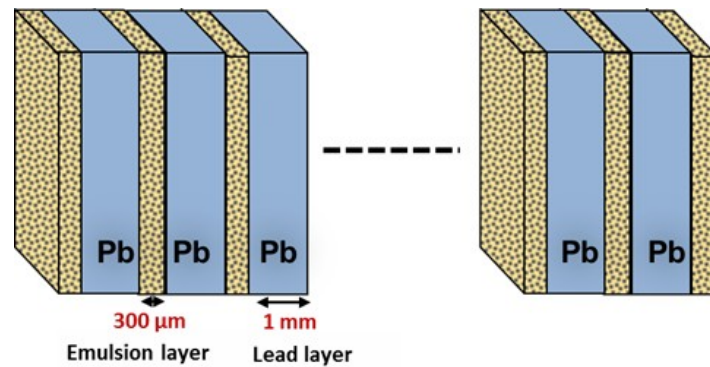


Figure 2.12: Scheme of the last section of the Emulsion Spectrometer, dedicated to the momentum measurement.

2.3 Experimental goals and requirements

The goal of the FOOT experiment is to measure the differential cross section of the nuclear fragmentation between the incoming beam and the target, to correctly identify the produced particles and introduce a new proton RBE model. In order to do that, the fragments characteristics measurements have to reach the precision levels listed in the following points:

- cross section of heavy fragments with a maximum uncertainty of $\sim 5\%$;
- energy differential cross section resolution $((d\sigma)/(dE))$ of the order of ~ 1 MeV/u;
- charge identification at the level of 2% - 3%;
- isotopic identification at the level of $\sim 5\%$.

To reach these goals, the FOOT experiment must fulfill some requirements about the detector performances. The quantities involved in the identification are the momentum p , the kinetic energy E_k , the energy released in a limited path $\frac{dE}{dx}$ and Time Of Flight (TOF) and have to reach this resolution:

- momentum resolution $\sigma(p)/p$ at the level of 4%;
- time of flight (TOF) resolution at the level of 70 ps;
- energy resolution $\sigma(E_k)/(E_k)$ at the level of 2%;
- $\sigma(\frac{dE}{dx})/(\frac{dE}{dx})$ at level of 2%;

For what concerns the emission angle of the fragments, the adoption of the inverse kinematics approach requires an accurate measurement of the particle angle in the laboratory frame, even though it is negligible for the application of heavy fragments in proton therapy. In fact, they have short ranges and release all the energy extremely close to the production site regardless of the initial angle. However, to correctly apply the inverse boost transformation, the emission angle resolution, with respect to the beam, should be of the order of few mrad. To achieve this resolution, the beam particles direction, before the target, and the fragment emission angle, after the target, must be tracked with an angular accuracy at the mrad level.

For light fragment measurements ($Z \leq 2$), on the other hand, it should be quite simple to achieve all the requirements due to the extremely high tracking precision that the nuclear emulsions can offer.

2.4 Fragments identification and measured quantities

Performing the inverse kinematic approach requires a high level of accuracy on measurements achieved through the experimental setup for heavy ion particles. To this end, the previously seen detecting devices are used in combination with each other to provide high precision and high granularity measurements.

In order to estimate as accurately as possible the parameters, FOOT adopts a global tracking reconstruction algorithm : the Kalman filter. This is a recursive algorithm method that allows the highest performances in track reconstruction and vertex reconstruction thanks to which is possible to determine the position, direction, momentum of the particles and the location of their production points.

Moreover, the high resolution required on the measurements is necessary in view of the application of the Lorentz boost.

The first step before the cross section evaluation is the identification of atomic (Z) and mass (A) numbers that define the fragment univocally.

Momentum and trajectory measurement The momentum and trajectory measurement is performed combining the information retrieved by the three tracking detectors “enclosing” the permanent magnets.

Kinetic Energy measurement The kinetic energy E_k of the fragments is reconstructed from the energy deposited while crossing all the heavy materials, typically the plastic scintillator and the calorimeter.

TOF measurement The Time Of Flight (TOF) of the particles is obtained from the interval time between the scintillator signal and the trigger-time supplied by the start counter. Moreover, the time necessary to the beam to cover the distance between the Start Counter and the target should be subtracted from the time measurement.

Velocity and β measurement The velocity (β) of the fragment is obtained from the measured particle’s TOF and from the length of the track (L), through the equation:

$$\beta = \frac{v}{c} = \frac{1}{c} \frac{L}{TOF} \quad (2.1)$$

Charge measurement The detector dedicated to the charge (Z) identification is the plastic scintillator that provides the measurement of the particle energy loss dE/dx , expressed by the Bethe-Block equation (formula 1.5) that depends on the particle charge:

$$\frac{dE}{dx} \propto z^2 f(\beta) \quad (2.2)$$

where $f(\beta)$ is function of the fragment velocity β .

Mass measurement Thanks to all these “primary” quantities it is possible to determine the mass m of the fragments and, consequently, the mass number A necessary, together with the Z , to identify unequivocally the fragments type. The values of m and A are proportional through the relation:

$$m = A \cdot u \quad (2.3)$$

where u is the atomic mass unit and is equal to $9,3828 \times 10^2 \text{ MeV}/c^2$.

FOOT is a redundant setup because it allows to reconstruct more quantities than necessary. For this reason, the evaluation of the mass number A can be performed in three different ways:

- using TOF and momentum:

$$A_1 = \frac{m}{u} = \frac{1}{u} \frac{p}{\beta c \gamma} \quad (2.4)$$

where $\gamma = 1/\sqrt{1 - \beta^2}$ is the Lorentz factor related to β .

- using TOF and kinetic energy:

$$A_2 = \frac{m}{u} = \frac{E_k}{u} \frac{1}{c^2(\gamma - 1)} \quad (2.5)$$

where E_k is the kinetic energy.

- using momentum and kinetic energy:

$$A_3 = \frac{p^2 c^2 - E_k^2}{2 \cdot u \cdot c^2 E_k} \quad (2.6)$$

Chapter 3

Inverse Kinematics

The peculiar aspect of the FOOT experiment is the cross section determination that is obtained with the employment of the Inverse Kinematics approach; this requires a precise measurement of the kinematic quantities in order to obtain a good resolution when considering the inverse frame (Section 2.3-2.4).

Another crucial aspect is a reliable fragment identification that is needed in order to distinguish the contributions arising from different isotopes.

Therefore, this chapter will deepen the fundamental aspects of this approach starting, in Section 3.1, with the presentation the fragmentation process by means of the ablation/abrasion model. Section 3.2 will face the different problems arising from the target and the projectile fragmentation, while the choice of the target material will be presented in Section 3.3. In Section 3.4 the mathematical formulation of the Inverse Kinematics approach will be shown. Section 3.5 will describe the kinematic characteristics of the produced fragments in the direct and inverse kinematics, respectively, and will underline the differences between the two approaches through the confrontation of plots of the fragments energy distribution.

3.1 Abrasion/Ablation Model for Nuclear Fragmentation

When beams have energies of several hundred MeV/u, nuclear fragmentation occurs in the collision with atomic nuclei and partial or total disintegration of the particles results from the beam/matter interaction [18].

Depending on the value of the impact parameter, the collisions can be central head-on, causing high fragment multiplicity of both projectile and target, or peripheral. For geometrical reasons the latter type, where the beam particle loses one or several nucleons, is the most frequent. It is characterized by a relatively small energy and momentum transfer, because not all the nucleons interact effectively, and only few fragment are produced.

In the peripheral collision, secondary particles can derive from the fragmentation of the incident particle that is caused by the projectile de-excitation after the collision, or can be produced by the target evaporation that follows the collision.

These nuclear interactions are well described by the two-step approach proposed by Serber [19], also called the *Abrasion/Ablation model*.

It is a simplification of the nucleus-nucleus collision and is divided in two stages with different time scales (Fig. 3.1). In the first phase, the *abrasion*, the nucleons, that are in the overlapping zone of the projectile trajectory and the target nuclei, interact and light particles are promptly emitted. In this process there is the formation of an excited quasi-projectile (colored in yellow in the figure) that follows the initial trajectory without relevant change of velocity, an excited quasi-target (blue) that slowly recoils and several excited light particles, collectively called *fire-*

ball (red). Other nucleons act like spectators and are only slightly affected by the collision. The abrasion process has a time scale typical of the strong interactions ($\approx 10^{-23}$ s). The second stage, described in this approach, is the *ablation* and it corresponds to the phase in which the fireball fragments de-excite going through various possible reactions that depends on energy and atomic number: nuclear evaporation, fission, Fermi-breakup or by mean of gamma emissions. The characteristic time scale for the ablation step varies between 10^{-16} s for excitation energies of 10 MeV and 10^{-21} s for energy values of 200 MeV.

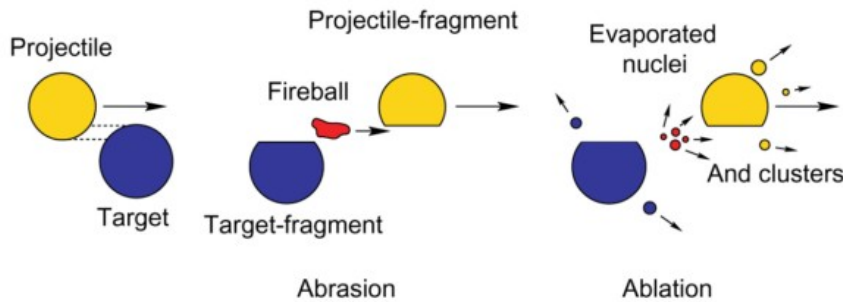


Figure 3.1: Schematic representation of the Abrasion/Ablation model for the nuclear fragmentation due to peripheral collisions of projectile and target nuclei.

Usually, target fragmentation gives a small contribution to the number of secondary particles produced in the collision when $Z > 2$, while is the only source of fragments when the beam is made out of protons.

On the other hand, considering Carbon ions, the major effects are due to the break up of the projectile particles.

3.1.1 Fragmentation Cross Sections

These kind of reactions are called *charge-changing reactions* because fragments of lower charge are produced in the collision [20].

The total reaction cross section σ_R , represents the probability that a collision takes place within the target. It is possible to quantify this probability within a certain covered distance x in the material and at a specific energy E , considering the cross section for inelastic collisions σ_{inel} and its correspondence to the difference between the total cross section and the elastic cross section ($\sigma_{el}(E)$):

$$\sigma_R = \sigma_{inel}(E) = \sigma_{tot} - \sigma_{el}(E) \quad (3.1)$$

Moreover, being N_0 the initial number of incoming particles, it is possible to evaluate the number of particles ($N(x)$) that survive after traversing a thickness x , through the formula:

$$N(x) = N_0 e^{-x/\lambda} \quad (3.2)$$

where λ represents the mean free path for a given cross section and is expressed as:

$$\lambda = \frac{M_{mol}}{N_A \rho \sigma_R} \quad (3.3)$$

with M_{mol} molecular mass, ρ density of the medium and N_A Avogadro's number.

The total reaction cross section, for a proton-nucleus reaction, is proportional to the area "seen" by the incoming projectile (πR^2); since the nucleus radius R is proportional to $A^{1/3}$, the relation between the cross section and the area is: $\sigma_R \propto A^{2/3}$. In the case of a nucleus-nucleus reaction,

on the other hand, it is possible to use the expression proposed by Bradt and Peters [21]:

$$\sigma_R = \pi r_0^2 (A_p^{1/3} + A_t^{1/3} - b_0)^2 \quad (3.4)$$

where A_p and A_t are the mass numbers of the projectile and the target, respectively, b_0 is the overlap or transparency parameter and r_0 is the nucleon radius.

From this expression is possible to deduct that given a projectile, for greater values of A_t an higher cross section is expected and an increase in the fragments production is foreseen.

In the specific case of Carbon-12 [9], the cross section for the production of a fragment ${}^A_Z X$, of atomic number Z and mass number A , is defined as:

$$\frac{d\sigma}{d\Omega}({}^A_Z X) = \frac{N_{{}^A_Z X} \cdot A_{target}}{N_{12C} \cdot \Omega \cdot \rho \cdot th \cdot N_A} \quad (3.5)$$

where $N_{{}^A_Z X}$ is the number of ${}^A_Z X$ fragments detected, N_{12C} is the number of incident carbon nuclei, Ω is the solid angle of the detector, $\rho \cdot th$ is the target area density (density (ρ) \times thickness (th)) and, in conclusion, A_{target} the target mass.

3.2 Projectile and Target fragmentation

In hadrontherapy beams of protons or heavy charged ions like ^{12}C are shoot against the tumor, within the patient tissues.

The human body is made up, for almost 99%, of Oxygen, Carbon, Hydrogen, Nitrogen, Calcium, and Phosphorus, and water constitutes $\sim 65\%$ of the body mass. For this reason, water had been in use as a human soft tissue equivalent since the beginning of radiation applications for treatment and research; experimental studies of the fragmentation of light ions in water or tissue-substitute materials already began being carried out in 1971 at Princeton. Medical Physics dosimetry protocols usually recommend the use of water phantoms to simulate scattering conditions in the patient body and to have an insight of what happens in the human tissues [22].

Since the main goal of the FOOT experiment is to achieve a precise evaluation of the proton RBE, some simulations of the collision between protons and water molecules were performed in order to estimate the ranges of the produced fragments [8]:

Fragment	E (MeV)	LET (keV/ μm)	Range (μm)
^{15}O	1.0	983	2.3
^{15}N	1.0	925	2.5
^{14}N	2.0	1137	3.6
^{13}C	3.0	951	5.4
^{12}C	3.8	912	6.2
^{11}C	4.6	878	7.0
^{10}B	5.4	643	9.9
^8Be	6.4	400	15.7
^6Li	6.8	215	26.7
^4He	6.0	77	48.5
^3He	4.7	89	38.8
^2H	2.5	14	68.9

Figure 3.2: Expected average physical parameters for target fragments produced in water by a 180 MeV proton beam.

Due to kinematic reasons, the fragments produced by the target fragmentation have a low energy and, consequently, a small range. On the contrary, the fragments derived from the projectile disintegration have high energy and long ranges.

This is confirmed by the data shown in Figure 3.2 from which is possible to see that the target fragments have a range of order of magnitude of micrometers and a low kinetic energy that cause all the secondary particles energy to be deposited locally. Therefore, it is not possible to analyze the outcomes of the collision between protons and a body-like target, since the fragments release all their energy within the target itself. Particles remain trapped within it and are not able to reach the opposite surface of the medium and interact with the rest of the setup. Therefore, it is not allowed any chance of detection.

A possible way to solve this problem would be the implementation of a thin target to facilitate the fragments emission, but this choice would introduce mechanical problems and, moreover, the rate of fragmentation would decrease greatly and would be very difficult to achieve a significant amount of data.

For this reason it was necessary to find an alternative approach to study the collision products and measure their dose deposition in the patient body. The opted solution was that of following the inverse kinematics approach, a *reverse geometry* technique showed for the first time in the work of Artemov [23].

When working with a light beam and a target composed of heavier particles, the projectile affects minimally the target nuclei and causes the creation of quasi-target products at rest

(target fragmentation). Therefore, it is not possible to detect the fragments because they remain confined in a small range. On the other hand, when the beam nuclei are heavier than the target ones, there is the projectile fragmentation and the main collision products are quasi-projectile particles that retain almost all the incident energy and can escape from the target.

This two behaviours are represented in the scheme of Figure 3.3.

Regarding the target fragmentation, the Inverse Kinematics approach operates switching the roles of the projectile and target leading to fragments that can be detected because ejected outside the target [24].

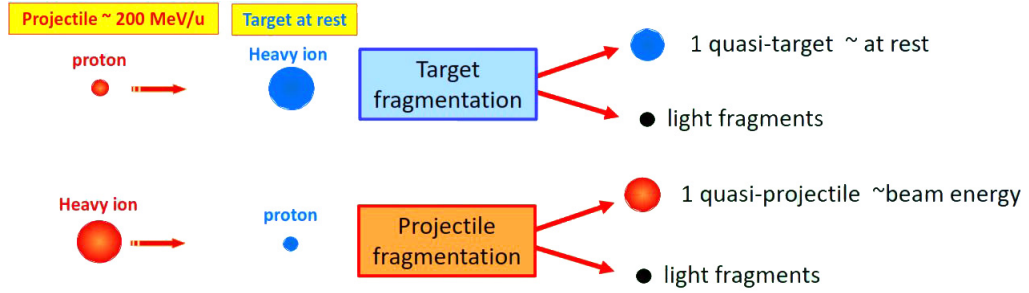


Figure 3.3: Fragments characteristics in direct and inverse kinematics.

Therefore, the application of this method calls for the employment of a beam of ^{12}C or ^{16}O (elements representative of the body composition) and a proton target. Moreover, in order to be able to use the Lorentz transformation, the kinetic energy per nucleon has to remain unchanged; hence, the beam will have the same kinetic energy of the previous proton beam (the one employed before the application of the inverse kinematics approach), but increased of a factor equal to the projectile mass. This allows also to maintain the same interaction probability that would, otherwise, decrease if the kinetic energy of the new beam had to be the same of the protons one.

The other FOOT goals, fragmentation of the projectile and radioprotection in space, that foresee the use of beams of heavy particles impinging always on the same target, do not require the use of the inverse kinematic. They do not present any detection problem because it is possible to measure the fragmentation cross section in a direct kinematic approach, since the fragmented particles acquire enough energy to escape from the material.

3.3 Target material

In order to satisfy the requirements imposed by the use of the inverse kinematics approach, the FOOT setup needs to implement a proton-rich target. The choice goes towards an Hydrogen target, but it is not convenient to work with a gas or a liquid because its use requires a special container that would introduce an additional uncertainty and, moreover, the number of collision would decrease.

Hence, all these difficulties have led to the employment of a technique already introduced in the GANIL experiment that consists in the application of the *combination method* [9]. In this approach, the differential cross section of a beam impinging against the Hydrogen target is obtained using the composite target of 2 mm thick layers of C_2H_4 and C (Fig. 3.4), and combining the respective cross sections as follows:

$$\frac{d\sigma}{d\Omega}(H) = \frac{1}{4} \cdot \left(\frac{d\sigma}{d\Omega}(\text{C}_2\text{H}_4) - 2 \frac{d\sigma}{d\Omega}(\text{C}) \right) \quad (3.6)$$

$$\frac{d\sigma}{dE_{kin}}(H) = \frac{1}{4} \cdot \left(\frac{d\sigma}{dE_{kin}}(\text{C}_2\text{H}_4) - 2 \frac{d\sigma}{dE_{kin}}(\text{C}) \right) \quad (3.7)$$

To check the validity of this approach, simulated data of the cross section on Hydrogen target were compared to data of the cross section obtained from the difference method. The results show a good agreement as can be seen in Figure 3.5.

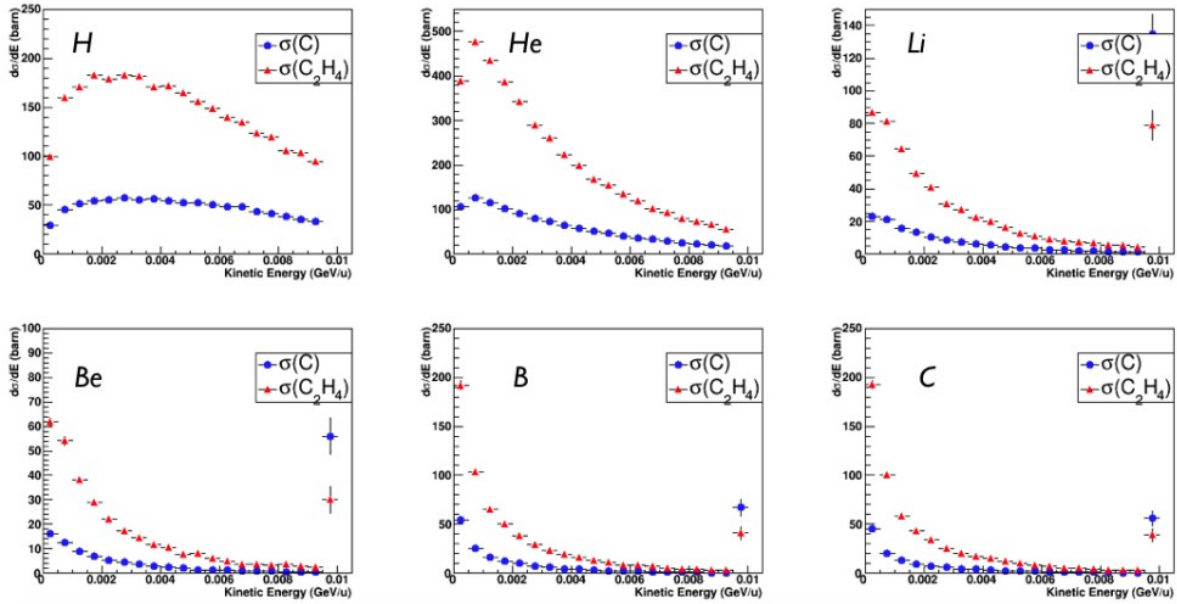


Figure 3.4: Energy differential cross-sections of different fragments in inverse kinematics. Results obtained for C_2H_4 and C targets are reported as blue dots and red triangles, respectively.

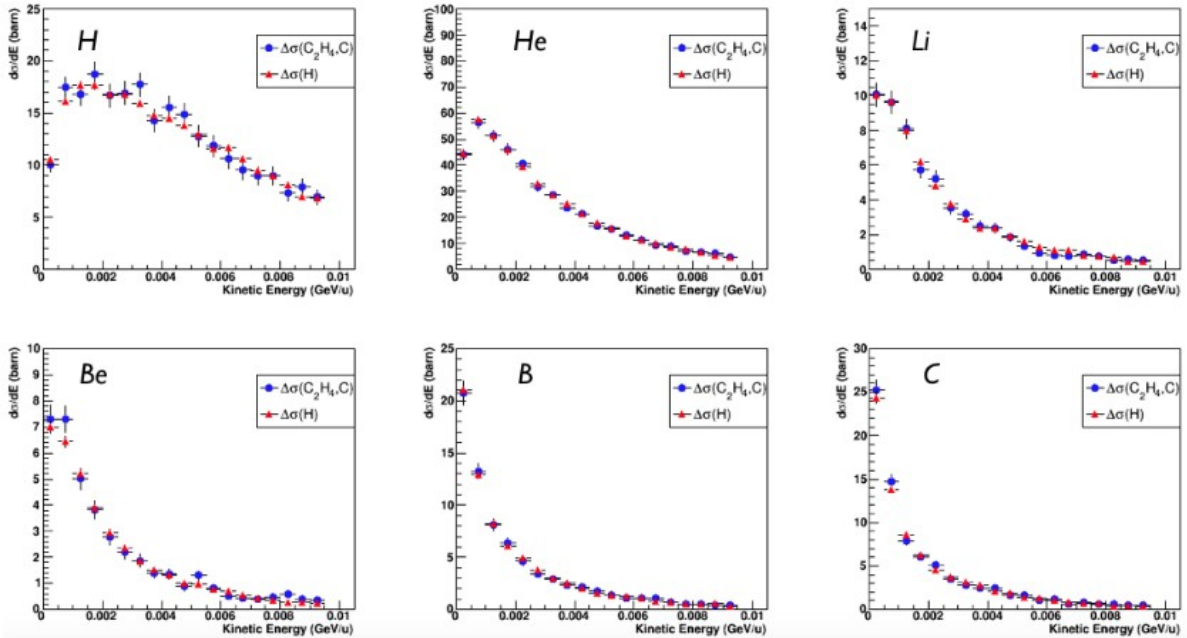


Figure 3.5: Energy differential cross-section of a 200 MeV/u ^{12}C beam on Hydrogen target in inverse kinematics. The estimations performed with the $\Delta\sigma(C_2H_4; C)$ and $\sigma(H)$ methods are reported as blue dots and red triangles, respectively.

A disadvantage of such method is that, since the researched cross sections are obtained by subtracting the cross sections of the two targets, the uncertainties will correspond to the quadratic sum of the uncertainties of both individual targets.

3.4 Mathematical Formulation of the Inverse Kinematics

The projectile particles employed in Hadrontherapy proceed at relativistic velocities and, consequently, the interaction with the target takes place in the same relativistic condition. To use the inverse kinematics approach is necessary to apply the *Lorentz transformation* that allows to switch from the laboratory frame to the “patient frame”.

It is a linear transformation that converts the coordinates between two inertial reference frames moving at constant velocity relative to each other. This mathematical tool may also include a rotation of space; in the absence of rotations the transformation is called a *Lorentz boost* (Fig. 3.6).

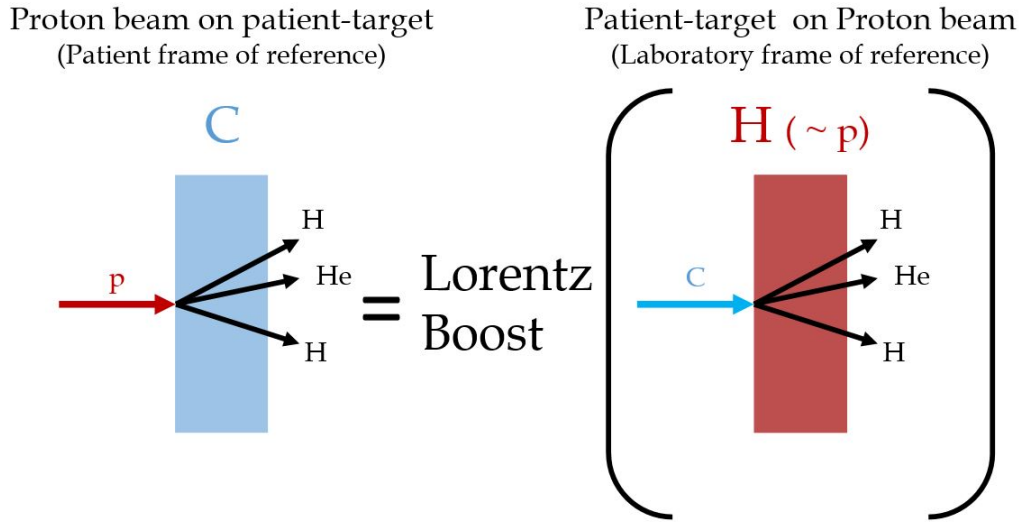


Figure 3.6: Scheme of the Lorentz transformation between the two reference frames.

The first step in the development of a relativistic kinematics is to determine the new coordinates transformation. To do so, it is necessary to consider two frames S and S' moving with constant relative velocity along the positive z axis, and such that their origins coincide at $t = 0$. S indicates the *laboratory frame* in which the incident beam, of heavy charged ions, impinges on the stationary hydrogen target. S' , instead, represents the *patient frame* in which target and projectile material are switched, meaning that the beam is made of protons and the target is composed of elements that constitutes the human body. Therefore, the coordinates that can be found experimentally are the one within the laboratory frame, while the coordinates denoted with a prime are measured in the patient frame.

Considering \mathbf{A} as a generic *four-vector* in the laboratory frame, it is defined as an object of four components:

$$\mathbf{A} = [a_0, a_1, a_2, a_3] = [a_0, \vec{a}] \tag{3.8}$$

where the first component is the temporal one and the other three indicate the spatial terms. Taken two inertial frames, S with x, y, z coordinates and S' with x', y', z' , is possible to apply the Lorentz transformation to the four-vector \mathbf{A} , in the S reference frame, and transform it in the four-vector \mathbf{A}' expressed in the “boosted” S' system (the patient frame where the target fragmentation takes place). The transformation can be written as:

$$\mathbf{A}' = \Lambda \mathbf{A} \tag{3.9}$$

where Λ_ν is a 4×4 matrix.

In the particular case of FOOT, the two reference frames motion is along a specific direction that can be identified with the z axis and the transformation is expressed as:

$$\begin{pmatrix} a'_0 \\ a'_1 \\ a'_2 \\ a'_3 \end{pmatrix} = \begin{pmatrix} \gamma & 0 & 0 & -\beta\gamma \\ 0 & 1 & 0 & 0 \\ 0 & 0 & 1 & 0 \\ -\beta\gamma & 0 & 0 & \gamma \end{pmatrix} \cdot \begin{pmatrix} a_0 \\ a_1 \\ a_2 \\ a_3 \end{pmatrix} = \begin{pmatrix} \gamma a_0 - \beta\gamma a_3 \\ a_1 \\ a_2 \\ -\beta\gamma a_0 + \gamma a_3 \end{pmatrix} \quad (3.10)$$

where $\beta = v/c$ and v (it corresponds to v_z) indicates the velocity of the S' system in relation to S , and $\gamma = 1/\sqrt{1 - \beta^2}$.

The matrix Λ of the transformation has the property that:

$$\Lambda^{-1}(\beta) = \Lambda(-\beta) \quad (3.11)$$

therefore, the inverse transformation is defined as:

$$\begin{pmatrix} a_0 \\ a_1 \\ a_2 \\ a_3 \end{pmatrix} = \begin{pmatrix} \gamma & 0 & 0 & \beta\gamma \\ 0 & 1 & 0 & 0 \\ 0 & 0 & 1 & 0 \\ \beta\gamma & 0 & 0 & \gamma \end{pmatrix} \cdot \begin{pmatrix} a'_0 \\ a'_1 \\ a'_2 \\ a'_3 \end{pmatrix} = \begin{pmatrix} \gamma a_0 + \beta\gamma a_3 \\ a_1 \\ a_2 \\ +\beta\gamma a_0 + \gamma a_3 \end{pmatrix} \quad (3.12)$$

Replacing the generic four-vector with the position one, the relations obtained from the direct approach can be written as:

$$ct' = \gamma(ct - \beta z) \quad (3.13)$$

$$x' = x \quad (3.14)$$

$$y' = y \quad (3.15)$$

$$z' = \gamma(z - \beta ct) \quad (3.16)$$

Considering the momentum \mathbf{P} it is also a four-vector, defined as:

$$\mathbf{P} = [E/c, \vec{p}] = [m\gamma c, m\gamma \vec{v}] \quad (3.17)$$

and its transformation is:

$$E'/c = \gamma(E/c - \beta p_z) \quad (3.18)$$

$$p'_x = p_x \quad (3.19)$$

$$p'_y = p_y \quad (3.20)$$

$$p'_z = \gamma(p_z - \beta E/c) \quad (3.21)$$

In the laboratory reference frame S , the four-vectors of the beam \mathbf{P}_1 and the target \mathbf{P}_2 are:

$$\mathbf{P}_1 = [E_1/c, \vec{p}_1] \quad (3.22)$$

$$\mathbf{P}_2 = [E_2/c, \vec{0}] = [m_2 c, \vec{0}] \quad (3.23)$$

3.4.1 Application

To facilitate the mathematical resolution, it is possible to use natural units and impose $c = 1$. Therefore, the Lorentz Boost is simply the subtraction of the β value of the beam from the measurements obtained through FOOT detectors.

This is allowed because the kinetic energy per nucleon remains unchanged in the inverse kinematics approach, hence, the β value is the same before and after the beam/target exchange.

Considering the main types of elements involved in Hadrontherapy and the maximum and minimum energies in the range of interest, it is possible to calculate the β involved in the Boost:

Beam	Mass	E_{kin} per nucleon	β
p	1 u = $9,3828 \times 10^2$ MeV/c ²	250 MeV	0.613607
4He	4 u	150 MeV/u	0.506623
		400 MeV/u	0.713054
${}^{12}C$	12 u	150 MeV/u	0.506623
		400 MeV/u	0.713054
${}^{16}O$	16 u	150 MeV/u	0.506623
		400 MeV/u	0.713054

3.5 Fragments characteristics in Direct and Inverse Kinematics

The necessity for the application of the Inverse Kinematics approach arises from the requirement to measure nuclear fragmentation cross sections of the target. The employment of protontherapy in actual medical treatments demands for the precise knowledge of the effect caused by these fragments in order to delineate an adequate treatment planning system. As mentioned in Section 3.2, it is not possible to detect the produced fragments because of their low velocity (hence, low kinetic energy) that prevents them to escape the target setup without any possibility of being detected.

In order to study the interaction of a proton beam with the human tissue (made up of heavy nuclei, typically C or O) it is necessary to switch the beam/target roles by analyzing the collision of a C or O beam on a proton target. Obviously, the method is valid only if the β (or, equivalently, the kinetic energy per nucleon) of the beams (protons in direct kinematics and C or O ions in the inverse kinematics) is the same. This request is necessary because the transformation matrix (see Section 3.4) depends only on the parameter β of the beam. In this way it is assured that the results obtained with a proton beam on a heavy nuclei target, in direct kinematics, is exactly the same of a heavy beam impinging on a proton target, in the inverse kinematics approach.

Direct Kinematics

Considering a simulated interaction of an Oxygen-16 beam of 200 MeV/u on a C_2H_4 target, 2 mm thick, the fragments are emitted with a slightly lower velocity than the incident beam and the kinetic energy distribution per nucleon appears to be peaked around the incident velocity value (Fig. 3.7).

The kinetic energy distribution becomes narrower with increasing number of nucleons, while lighter fragments present a smeared configuration. This behaviour is caused by the fragments mass that decreases and becomes more similar to that of the protons within the target; consequently, the fragments are more likely to interact with the target resulting in a change of the fragments velocity.

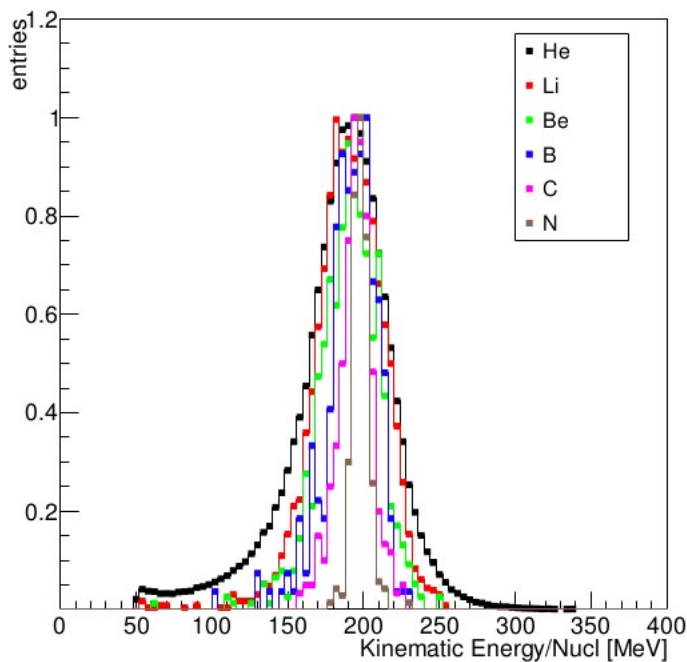


Figure 3.7: Fragments kinetic energy distribution per nucleon, obtained through a simulated interaction between an Oxygen-16 beam of 200 MeV/u and a C_2H_4 target.

The most recurring fragments produced in the collision are: ^1H , D, T, ^3He , ^4He , ^7Li , ^9Be , ^{11}B , ^{12}C , ^{14}N , ^{16}O . The Figure 3.8 shows their kinetic energy; it increases when the number of nucleons becomes greater.

The energies of the fragments can reach the order of some GeV.

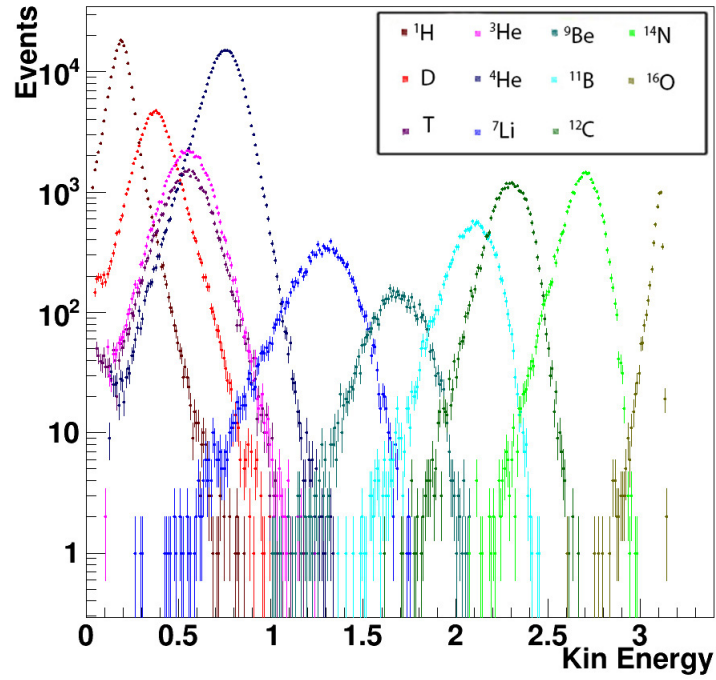


Figure 3.8: Kinetic energy distribution of fragments, obtained through a simulated interaction between an Oxygen-16 beam of 200 MeV/u and a C_2H_4 target. The kinetic energy is expressed in GeV.

The plots for each fragment are shown in Figures 3.9 and 3.10 and they confirm what told until this point. The peak appears in correspondence of $200 \text{ MeV} \times$ the number of nucleons, while the distributions are narrower for heavier fragments.

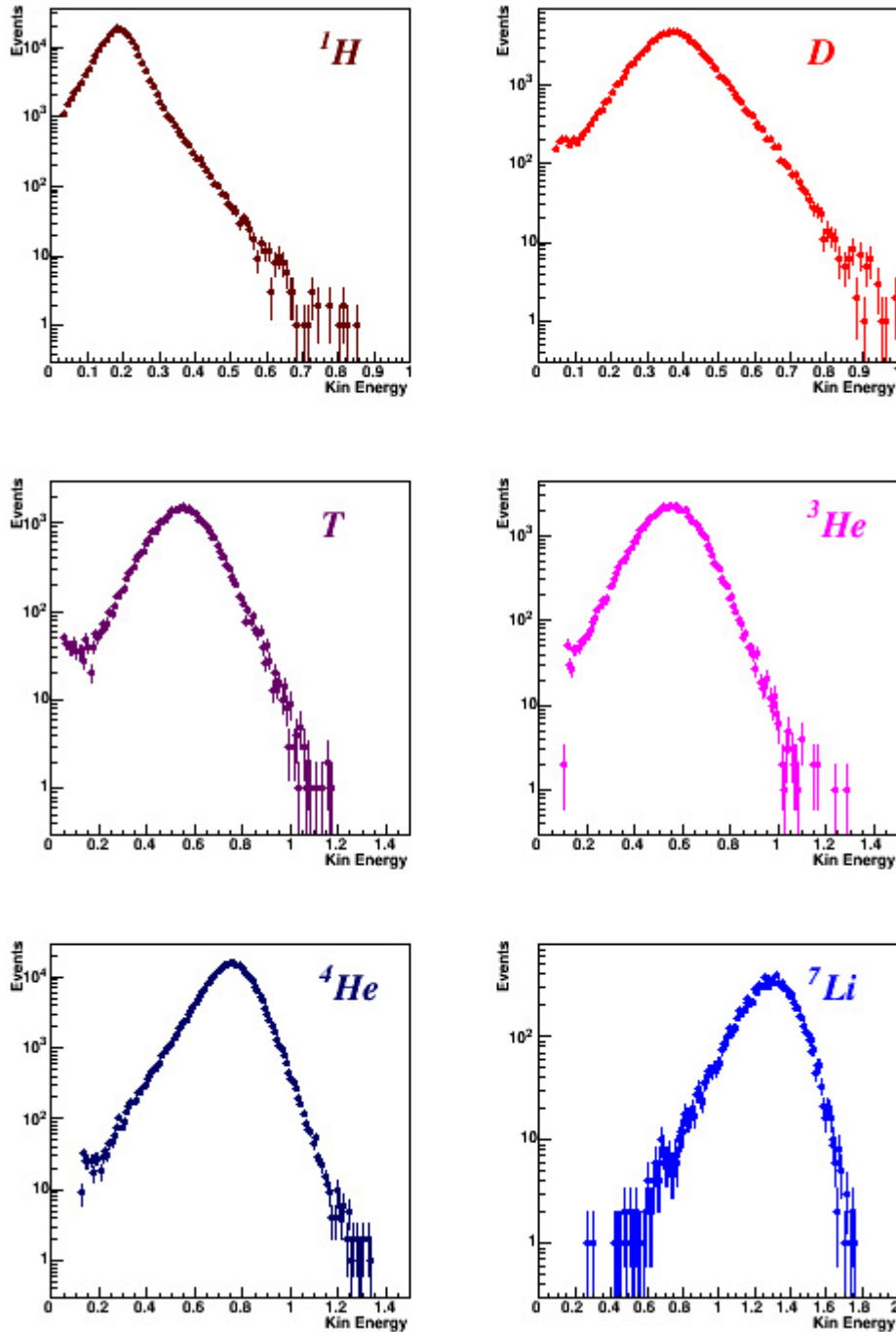


Figure 3.9: Kinetic energy distribution of ^1H , D , T , ^3He , ^4He , ^7Li in direct kinematics (obtained through a simulated interaction between an Oxygen-16 beam of 200 MeV/u and a C_2H_4 target). The kinetic energy is expressed in GeV.

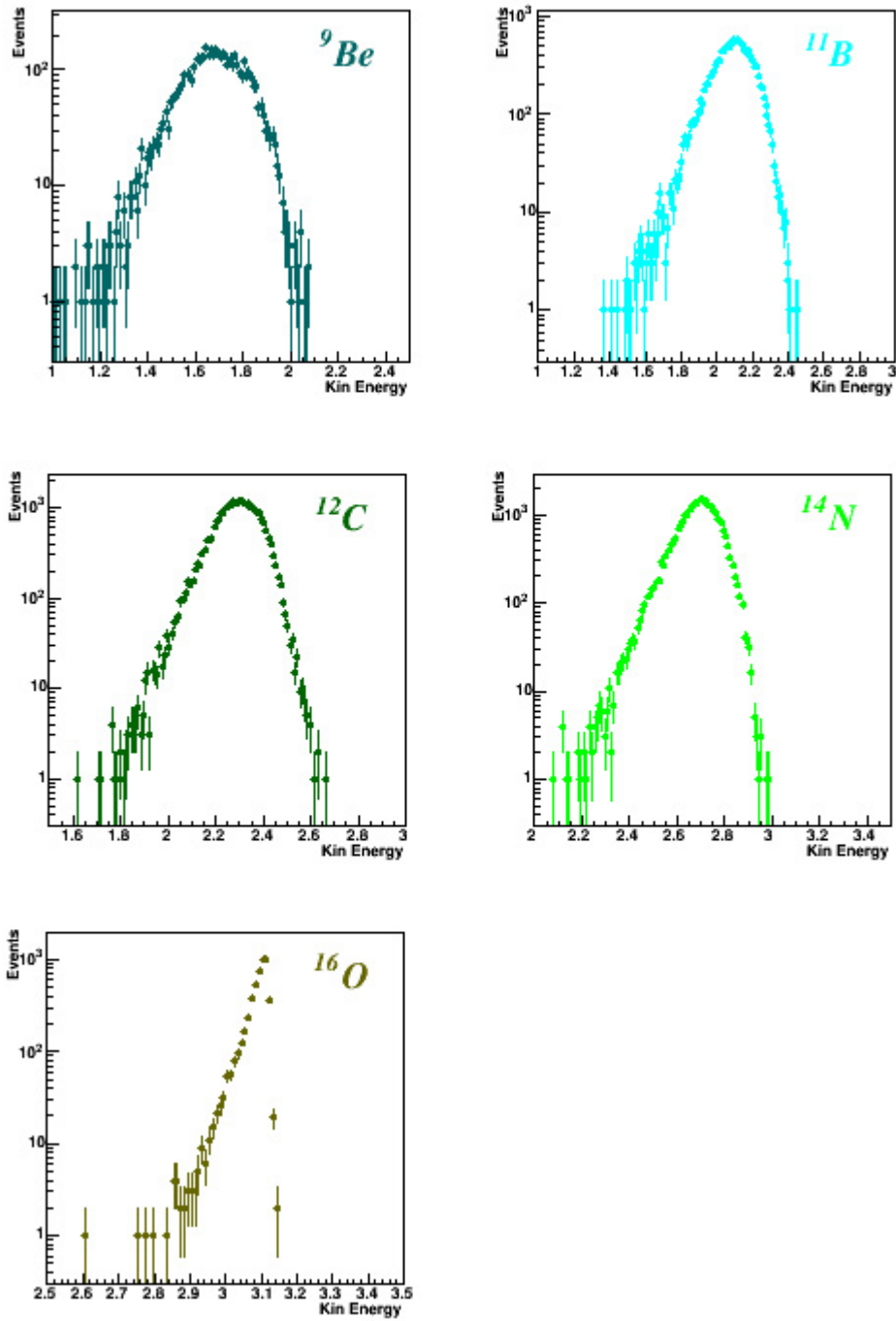


Figure 3.10: Kinetic energy distribution of ${}^9\text{Be}$, ${}^{11}\text{B}$, ${}^{12}\text{C}$, ${}^{14}\text{N}$, ${}^{16}\text{O}$ in direct kinematics (obtained through a simulated interaction between an Oxygen-16 beam of 200 MeV/u and a C_2H_4 target). The kinetic energy is expressed in GeV.

The angular distribution of the heavier produced fragments, in direct kinematics, is inside $\pm 10^\circ$ around the beam direction, while it is really spread out for lighter fragments as a consequence of multiple Coulomb scattering (Fig. 3.11).

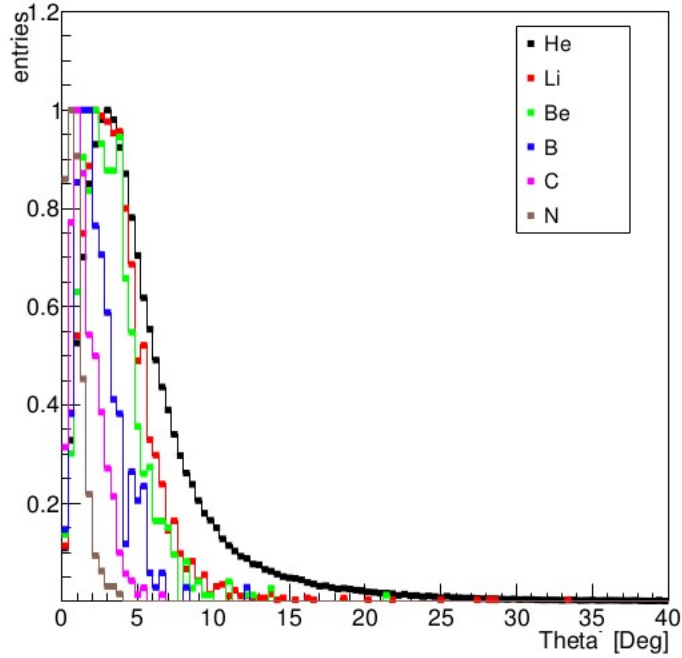


Figure 3.11: Angular distribution of fragments, obtained through a simulated interaction between an Oxygen-16 beam of 200 MeV/u and a C_2H_4 target.

This explains the reason behind the implementation, in the FOOT experiment, of two different setups (see Section 2.2): the electronic setup for the detection of the heavy fragments and the emulsion chamber for the light fragments measurement.

Inverse Kinematics

As expected, the kinetic energy distribution of the fragments in inverse kinematics is limited to a range of few MeV (Fig. 3.12) that prevents the fragmentation products to escape the target and to be detected.

The lighter fragments have a different distribution that extends to higher energies as a consequence of the smeared distribution that they had in direct kinematics. In fact, it is crucial to have high resolutions on the kinematic quantities in order to appreciate small differences in the distribution in the inverse kinematics approach. If the measurements in direct kinematics are not precise enough, the inaccuracy propagates in the inverse kinematics case affecting most of the results.

In order to obtain cross section measurements with a resolution at the level of 5%, the precision required for the kinetic energy has to be of 1-2 MeV in the inverse kinematics approach.

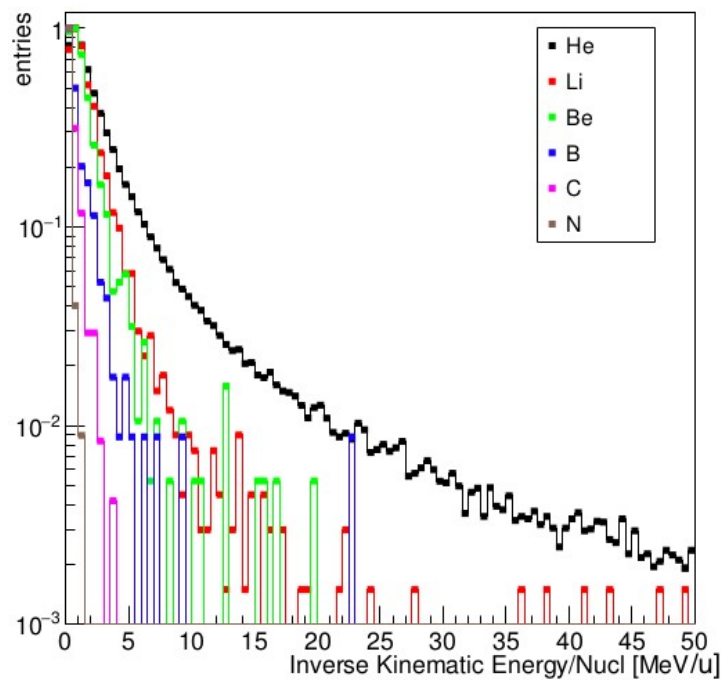


Figure 3.12: Fragments kinetic energy distribution per nucleon, obtained through a simulated interaction, in inverse kinematics, between an Oxygen-16 beam of 200 MeV/u and a C_2H_4 target.

The kinetic energy distribution (Fig. 3.13) presents a similar trend:

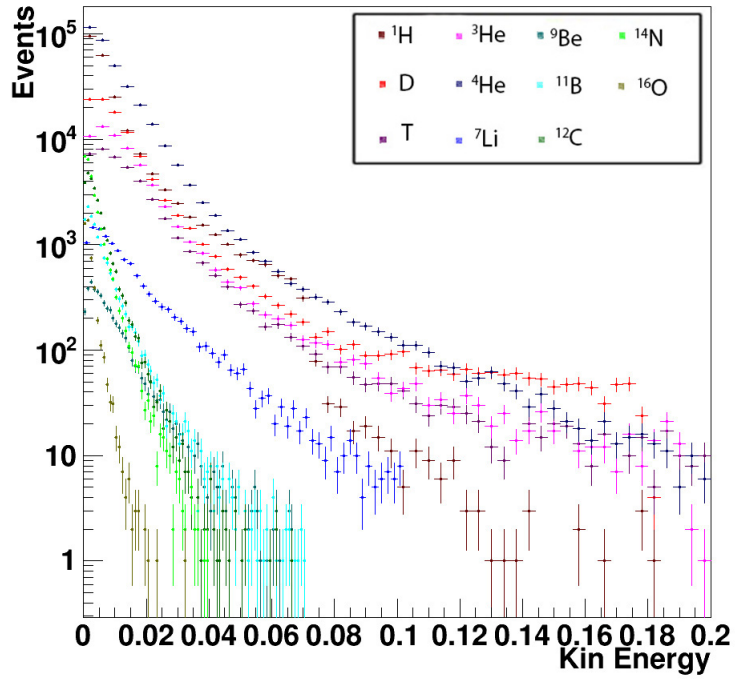


Figure 3.13: Kinetic energy distribution of fragments, obtained through a simulated interaction, in inverse kinematics, between an Oxygen-16 beam of 200 MeV/u and a C_2H_4 target.

Considering each single fragment (Fig. 3.14- Fig. 3.15) the distributions are:

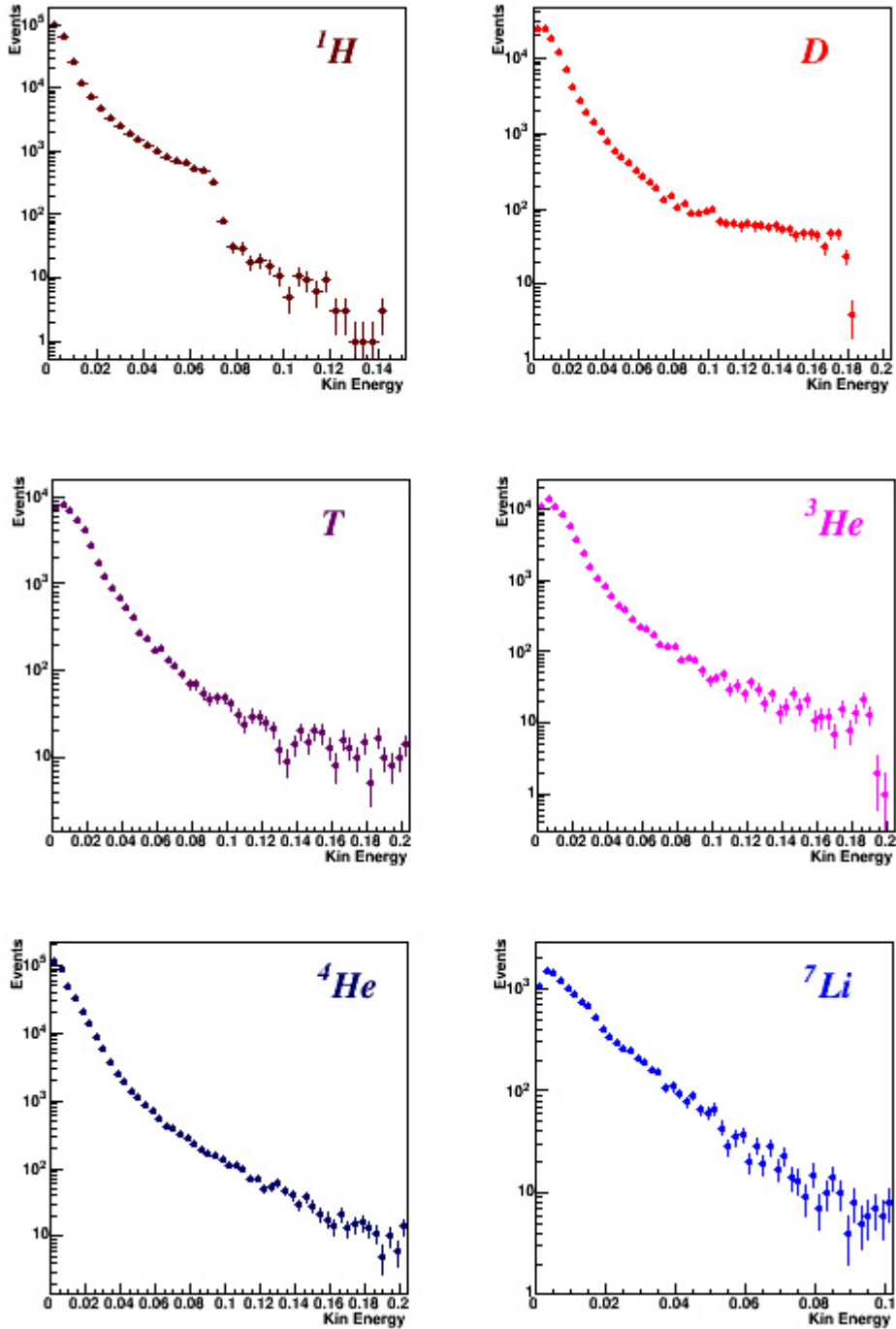


Figure 3.14: Kinetic energy distribution of ¹H, D, T, ³He, ⁴He, ⁷Li in inverse kinematics (obtained through a simulated interaction between an Oxygen-16 beam of 200 MeV/u and a C₂H₄ target). The kinetic energy is expressed in GeV.

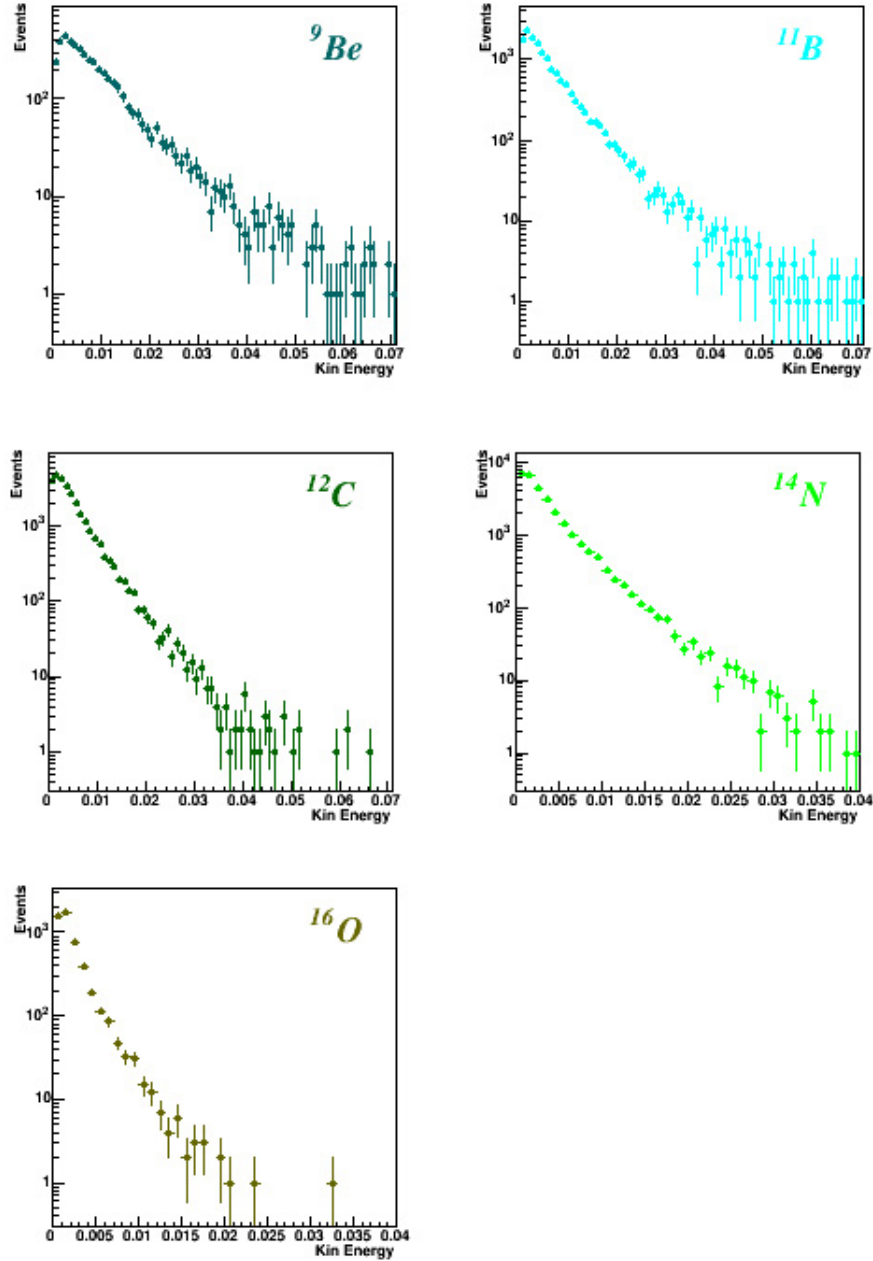


Figure 3.15: Kinetic energy distribution of ${}^9\text{Be}$, ${}^{11}\text{B}$, ${}^{12}\text{C}$, ${}^{14}\text{N}$, ${}^{16}\text{O}$ in inverse kinematics (obtained through a simulated interaction between an Oxygen-16 beam of 200 MeV/u and a C_2H_4 target). The kinetic energy is expressed in GeV.

In the inverse kinematics approach the angular distribution of the produced fragments loses all its meaning. In fact, due to the very low value of the kinetic energy distribution and, consequently, to the very small range in the human tissue, it has, from a therapeutic point of view, a negligible influence on the fragments path since it changes it of only few micrometers.

Conclusions

The goal of the FOOT (FragmentatiOn Of Target) experiment is to improve the knowledge of the nuclear processes that take place during the beam/patient interactions in the hadrontherapy treatments. The collisions of the therapeutic beams with the nuclei of the human body cause the production of fragments that can release their energy outside of the tumor volume. The experiment was designed to measure the fragmentation cross section in order to accurately evaluate the dose deposition in the patient's body.

The kinematic characteristics of the produced fragments depend on the nuclear fragmentation process. In particular, if the fragments derive from the beam fragmentation, they acquire almost all the initial kinetic energy of the beam and can reach the detectors. On the contrary, if they are produced by the target fragmentation, their kinetic energy and, consequently, their ranges are small (tens of micrometers), preventing the possibility of overstepping the target thickness and to be detected.

In order to study the target fragmentation the strategy of the FOOT experiment is to use the Inverse Kinematics approach. With this technique is possible to exchange the roles of beam and target causing the beam fragmentation (instead of the target) and promoting the creation of secondary fragments with high kinetic energy and longer ranges. In this way it is possible to study the fragmentation of the human nuclei, caused by a proton beam, through the implementation of an enriched hydrogen target and using Carbon or Oxygen beams.

This approach, despite being used in few experiments in the past, has guaranteed satisfactory results. The validity of this method has been faced in this thesis analyzing simulated data and generating the kinematics quantities of the most produced fragments in both inverse and direct approaches. From the comparison of the kinetic energy distributions in the two approaches, it is evident the importance of achieving precise measurements in direct kinematics in order to not affect the results in the inverse one. Therefore, to obtain cross section measurements with a resolution level of 5%, the precision required for the kinetic energy has to be of 1-2 MeV in the inverse kinematics approach.

Bibliography

- [1] <http://pathology.jhu.edu/pc/BasicTypes1.php?area=ba>
- [2] A. Schipler, G. Iliakis, *DNA double-strand-break complexity levels and their possible contributions to the probability for error-prone processing and repair pathway choice*, *Nucleic Acids Research*, vol. 41, no. 16, pp. 7589–7605, 2013.
- [3] O. Desoukya, G. Zhouba, *Biophysical and radiobiological aspects of heavy charged particles*, *Journal of Taibah University for Science*, no. 10, pp. 187-194, 2016.
- [4] H. Song, S. Senthamizchelvan, R. F. Hobbs, G. Sgouros, *Alpha Particle Emitter Radiolabeled Antibody for Metastatic Cancer: What Can We Learn from Heavy Ion Beam Radiobiology?*, *Antibodies*, no. 1, pp. 124-148, 2012.
- [5] D. Schardt, T. Elsasser, D. Schulz-Ertner, *Heavy-ion tumor therapy: Physical and radiobiological benefits*, *Reviews of Modern Physics*, vol. 82, pp. 383-425, 2010.
- [6] <http://enlight.web.cern.ch/what-is-hadron-therapy>
- [7] O. Jäkel, C. P. Karger, J. Debus, *The future of heavy ion radiotherapy*, *Med Phys.*, vol. 35, no. 12, pp. 5653-63, 2008.
- [8] F. Tommasino, M. Durante, *Proton Radiobiology*, *Cancers*, no. 7, pp. 353-381, 2015.
- [9] J. Dudouet, D. Juliani, J.C. Angélique, B. Braunn, J. Colin *et al.*, *Double differential fragmentation cross-section measurements of 95 MeV/u ^{12}C on thin targets for hadrontherapy*, *Phys. Rev. C*, American Physical Society, vol. 88, no. 2, 2013.
- [10] M. Toppi *et al.*, *Measurement of fragmentation cross sections of ^{12}C ions on a thin gold target with the FIRST apparatus*, *Phys. Rev. C*, vol. 93, no. 6, p. 064601, 2016.
- [11] G. De Lellis *et al.*, *Measurement of the fragmentation of Carbon nuclei used in hadrontherapy*, *Nucl. Phys. A*, vol. 853, no. 1, pp. 124–134, 2011.
- [12] F. Tommasino *et al.*, *New ions for therapy*, *Int. J. Part. Ther.*, vol. 2, no. 3, pp. 428–438, 2015.
- [13] B. Knäusl *et al.*, *Can particle beam therapy be improved using helium ions? - a planning study focusing on pediatric patients*, *Acta Oncol.*, vol. 55, no. 6, pp. 751–759, 2016.

- [14] R. Grün *et al.*, *Assessment of potential advantages of relevant ions for particle therapy: A model based study*, Med. Phys., vol. 42, no. 2, pp. 1037–1047, 2015.
- [15] M. Durante, F. Cucinotta, *Physical basis of radiation protection in space travel*, Rev. Mod. Phys., vol. 83, no. 4, p. 1245, 2011.
- [16] G. De Lellis *et al.*, *Nuclear emulsions, Elementary Particles: Detectors for Particles and Radiation*, vol 21B, Springer, 2011.
- [17] G. De Lellis, S. Buontempo, *Emulsion Cloud Chamber technique to measure the fragmentation of a high-energy carbon beam*, J. Instrum, vol 2, p P06004, 2007.
- [18] G. J. Russell, *Spallation Physics - An Overview*, ICANS - XI International Collaboration on Advanced Neutron Sources, KEK, Tsukuba, October 22-26, 1990.
- [19] R. Serber, *Nuclear Reactions at High Energies*, Phys.Rev., vol. 72, no. 11, pp. 1114-1115, 1947.
- [20] I. Schall, D. Schardt *et al.*, *Charge-changing nuclear reactions of relativistic light-ion beams ($5 \leq Z \leq 10$) passing through thick absorbers*, Nuclear Instruments and Methods in Physics Research B, 117, pp. 221-234, 1996.
- [21] L. Sihver, C. H. Tsao *et al.*, *Total reaction and partial cross section calculations in proton-nucleus ($Z_t \leq 26$) and nucleus-nucleus reactions (Z_p and $Z_t \leq 26$).*, Phys. Rev. C, vol. 47, pp. 1225–1236, 1993.
- [22] R. Ravichandran, *Artificial body fluid as tissue substitute for radiotherapy beam analysis: A theoretical evaluation of its electron density information*, J. Med. Phys., vol. 42(3), pp. 191–193, Jul-Sep 2017.
- [23] K. P. Artemov *et al.*, *Effective method of study of α cluster states*, Sov. J. Nucl. Phys., vol 52, no. 3, pp. 408-411, 1990.
- [24] J Walshe *et al.*, *The thick target inverse kinematics technique with a large acceptance silicon detector array*, Journal of Physics: Conference Series, no. 569, 2014.